Novel coupled permafrost-forest model revealing the interplay between permafrost, vegetation, and climate across eastern Siberia

Stefan Kruse[1*], Simone M. Stuenzi[1,2], Julia Boike[1,2], Moritz Langer[1,2], Josias Gloy[1], Ulrike Herzschuh[1,3,4]

1 Alfred Wegener Institute Helmholtz Centre for Polar and Marine Research, 14473 Potsdam, Germany
2 Department of Geography, Humboldt Universität zu Berlin, 12489 Berlin, Germany
3 Institute of Environmental Sciences and Geography, University of Potsdam, 14476 Potsdam, Germany, and
4 Institute of Biochemistry and Biology, University of Potsdam, 14476 Potsdam, Germany

Correspondence to Stefan Kruse: stefan.kruse@awi.de

Abstract. Boreal forests of Siberia play a relevant role in the global carbon cycle. However, global warming threatens the existence of summergreen larch-dominated ecosystems likely enabling a transition to evergreen tree taxa with deeper active layers. Complex permafrost-vegetation interactions make it uncertain whether these ecosystems could develop into a carbon source rather than continuing atmospheric carbon sequestration under global warming. Consequently, shedding light on the role of current and future active-layer dynamics and the feedbacks with the apparent tree species is crucial to predict boreal forest transition dynamics, and thus for aboveground forest biomass and carbon stock developments. Hence, we established a coupled model version amalgamating a one-dimensional permafrost-multilayer forest land-surface model (CryoGrid), with LAVESI, an individual-based and spatially explicit forest model for larch species (*Larix* Mill.), extended for this study by including other relevant Siberian forest species and explicit terrain.

Following parametrization, we ran simulations with the coupled version to the near future to 2030 with a mild climate-warming scenario. We focus on three regions, covering a gradient of summergreen forests in the east at Spasskaya Pad to mixed summergreen-evergreen forests close to Nyurba, and the warmest area at Lake Khamra in the south-east of Yakutia, Russia. Coupled simulations were run with the newly implemented boreal forest species and compared to runs allowing only one species at a time, as well as to simulations using just LAVESI. Results reveal that the coupled version corrects for overestimation of active-layer thickness (ALT) and soil moisture and large differences in established forests are simulated. We conclude that the coupled version can simulate the complex environment of central Siberia reproducing vegetation patterns making it an excellent tool to disentangle processes driving boreal forest dynamics.

1 Introduction

Boreal forests cover vast areas of the northern hemisphere with strong gradients in climatic conditions and environments. They established in the northern hemisphere after the last glacial maximum, leaving only a thin stretch in the north bordering the Arctic Ocean of pristine tundra areas (Mamet et al., 2019, Bonan, 2008, MacDonald et al., 2010). Anthropogenic climate

warming is leading to the relaxation of warmth-deficit limits at the northern margins and hence invasion of the tundra at an as yet unclear rate (Berner, 2013, Reese et al., 2020). At the same time, large parts of boreal forests, especially in central Siberia, are prone to droughts and increasing disturbances (such as fires) potentially driving a forest transition from deciduous species to evergreen taxa (Bonan, 2008, Herzschuh 2020). Accordingly, the albedo and further ecosystem components/feedbacks will

5 change and due to the large size of such boreal forests, this is likely to have a positive feedback effect on climate warming (Bonan, 2008). However, the involved forest dynamics and interactions with the atmosphere and soil need to be considered in sufficient detail to forecast projections that are more realistic and to understand better the consequences for the ecosystems of Siberia (Kirpotin et al., 2021).

Forest modelling is typically done globally including the carbon cycle/permafrost etc. but individuals and all life-history stages

10 need to be considered for a precise simulation. Modern global models such as LPJ-GUESS (Zhang et al., 2013) include individual models. They are used to show that forests will change and advance north. However, migration lags are typically not represented and only climate envelopes serve for the distribution of plant functional types (PFTs). Dispersal processes and complexities have recently been recognized (Snell 2014, Snell & Cowling 2015, Lehsten et al., 2019) but are not yet used as standard for simulations. Further, most modelling schemes still start with established trees, which makes them more general

15 and computationally effective for a global application but at the cost of losing important detail for ecosystem responses (see discussion in Kruse et al., 2016). Also, the use of representative grid cells on a large grid without considering landscape will cause deviations to an extent that is unclear as to whether the impact on results is large and significant or not. Individual based models (IBMs) could help here as they have sufficient detail of represented species/ecosystems but applications are therefore only possible on landscapes not continents (Grimm & Railsback, 2005, DeAngelis & Mooij, 2005). Nevertheless, they are the

20 best tools to understand a system and develop general responses that can then inform or guide global model development. Further, neither a radiative transfer scheme through a multilayer canopy nor detailed representation of permafrost are included in typical simulation approaches.

Here, we aim at creating a model system that can accurately assess detailed thermal and hydrological fluxes between permafrost

25 and forest cover as recently developed by Stuenzi et al. (2021a, 2021b). It will include a dynamic vegetation model, which has a full life-cycle to allow intraspecies and interspecies interactions at all stages (seed–seedling–mature tree) leading to non-linear behaviour of population dynamics as well as resolving a 3-dimensional landscape that is available for Siberian treeline areas developed by Kruse et al. (2016, 2019a, 2019b).

2 Methods

2.1 The 2D vegetation model LAVESI

2.1.1 Description and updates

The *Larix* vegetation simulator (LAVESI) is an individual-based spatially explicit model that simulates larch stand dynamics
5   (Kruse et al, 2016; Kruse et al, 2018). Monthly temperatures of the coldest (January) and warmest (July) months and
precipitation series can force this model. In addition, 6-hourly data on wind speed and direction are needed to simulate seed
distribution and tree reproduction, growth, and death (Kruse et al., 2019b; Kruse et al., 2018; Kruse et al., 2016).

2.1.2 Addition of landscape sensing

Data from the digital elevation model (DEM) TanDEM-X 90 m was downloaded from the web service provided by the German
10   Aerospace Center (DLR https://download.geoservice.dlr.de/TDM90/; Krieger et al., 2007). Subsequently, the tiles were
reprojected to the corresponding UTM zone of the focus areas (Khamra N49, Nyurba N50, Spasskaya N52). All tiles were
merged for each subzone and resampled by linear interpolation from 90 m to 30 m resolution using functions from the "raster"
package in R (Hijmans, 2020). The results were imported in SAGA GIS version 2.3.2 (Conrad et al., 2015) and subjected to a
basic terrain analysis tool using the standard parameters. The resulting rasters were water masked using the cloud-based
15   geospatial data analysis platform Google Earth Engine (GEE, Gorelick et al., 2017) to assess Sentinel-2 imagery between 1st
May 2018 and 15th October 2018 with a cloud cover of less than 20% and thresholds manually set for spectral band B12 (2190
nm) until all water was masked out by comparing them to an RGB composite image. The DEM along with slope angle and
terrain water index (TWI, moisture content) were cropped to 510x510 m (260,100 m²) areas for this study and exported as
plain text files for import into LAVESI.
20   LAVESI reads this data provided in 30 m resolution and interpolates linearly from the closest four grid cells for each 20 cm
grid tile of the environment grid. Based on empirical relationships of forest presence for combinations of slope angle and TWI
established in a study by Shevtsova et al. (in prep, 2021), an environment growth impact factor (*Envirgrowth*, 0–1) is calculated
for each tile and tree diameter growth at this position is reduced accordingly (Eq. 1, Appendix A).

$$Envirgrowth_i = \frac{-0.045999 * TWI_i + 0.994066}{2} + \frac{0.85654 * e^{-0.5 * (Slope_i - 8.78692)^2 / 6.90743^2}}{2} \qquad (1)$$

25   where TWI_i is the interpolated terrain water index of the 20x20 cm² environmental grid cell i, and $Slope_i$ is the slope angle of
the same grid cell i.

Seed dispersal has been improved. Seeds can now only be dispersed to places which are at the same or lower elevation than
the release height in the terrain.

2.1.3 Addition of species and estimating leaf area index (LAI)

Further species were added to the existing model presented in Kruse et al. (2016). To add a fast forward implementation of species in LAVESI, we modified the code so that the program can be started with either one or all species in a mix simultaneously. The species are numbered (integer values), which are used internally to assess species-related variables (Table

5   1, further variables in Appendix B, Table B1) when called for in the functions as necessary. Therefore, the code is independent from the species and allows adding species or functional types simply by adding a new line in the new *specieslist.csv* in the main folder of LAVESI.

For this study, we analysed field data from the Chukotka and central Yakutia 2018 expedition in the same way as we did for

10   Chukotka (Biskaborn et al., 2019, Kruse et al., 2019a). In the area of central Yakutia, species belonging to the Pinaceae family form the forests. From these, two deciduous boreal forest tree species were sampled, *Larix cajanderi* Mayr. (LACA) and *Larix gmelinii* (Rupr.) Rupr.*,* (LAGM), and three evergreen species, *Picea obovata* Ledeb. (PIOB), *Pinus sibirica* Du Tour (PISI), and *Pinus sylvestris L.* (PISY) (Kruse et al., 2019a). While the two larch species are best adjusted to the harsh environment of Northeast Siberia, and are able to grow on shallow active layers above permafrost, they differ mainly in their frost hardiness

15   and the species LACA can even endure colder temperatures in winter (Table 1). PIOB is a competitor for *L. gmelinii* growing at similar environmental conditions, however preferring deeper thawed active layers of minimum of 200 cm. On well-drained sites, PISY grows well and outcompetes the other species. In milder environments, LASI and PISI grow on similar sites as LAGM and PIOB.

20   Tree-ring width data were established from tree discs and cores collected from sites close to Lake Khamra and from the region Nyurba. The discs and tree cores were prepared by standard dendroecological processing steps: (1) sanding with progressively finer paper until tree rings are clearly visible, (2) making high-resolution images for a track with a binocular and attached camera, (3) detecting rings with CooRecorder (Cybis Elektronik & Data AB) and cross-dating, and (4) exporting individual tree-ring chronologies (more details in Kruse et al., 2020). Tree-ring width data per species were then imported to R using the

25   dplR package (Bunn et al., 2020) and regression models were set up with the gnls-function from the nlme package (Pinheiro et al., 2019). For each species, we extracted the median of the loess-smoothed (span=1.5) yearly growth increase of individual trees and set up a generalized least squares regression using a nonlinear model. This was successful for LACA, LAGM, and PIOB, but not for PISI and PISY due to small sample sizes, where current values of PIOB are used as a first estimate (Table 1). For each tree in the simulation, the maximum actual growth can be estimated with the following equation.

30   $$TRW_{Species\ j, year\ t} = exp(gdbasalconst + gdbasalfac * t + gdbasalfacq * t^2) \tag{2}$$

where TRW is the tree-ring width for species *i* at one year depending on the fitted parameters gdbasalconst, gdbasalfac, and gdbasalfacq.

Biomass data were prepared following the protocol of Shevtsova et al. (2020) and allometric relationships were established to empirically estimate the leaf area (LA) from total leaf biomass for each tree (Eq. 3), followed by a log-log linear regression forced to pass through the origin employing the basal diameter as explanatory variable (Eq. 4). To estimate the LA for each

5 tree, we used specific leaf area (SLA) parameters to translate from the dry weight of needles to leaf area (Eq. 3). For each species, the SLA was extracted from literature values: SLA_{LAGM} = 120 cm² g⁻¹ (Xian-kui et al., 2015), which was also used for the closely related sister species LACA, SLA_{PIOB} = 50 cm² g⁻¹ (Konôpková et al., 2020), SLA_{PISY} = 50 cm² g⁻¹ (extracted from the most recent source Błasiak et al., 2021, although other values are reported, 34 cm² g⁻¹ in Reich et al., 1998, 40 cm² g⁻¹ in Mencuccini & Bonosi, 2001). For PISI no source for SLA values was found and we assume it is similar to PISY.

10 $$LA_{Tree\ i,Species\ j} = BM_{dry\ needle}SLA_{Species\ j}/100 \tag{3}$$

where *BM* is the biomass of tree *i* in g, and *SLA* is the specific leaf area for species *j*.

$$\log\left(LA_{Tree\ i,Species\ j}\right) = a * \log(DB_{Tree\ i}) + 0 \tag{4}$$

15 where *a* is the slope of the linear model fit and *DB* is the basal diameter of the tree *i*. for species *j*

During simulations runs with LAVESI, the LA for each individual tree is estimated based on the fitted linear regression model using the following equation.

$$\widehat{LA_{i,j}} = exp(a * log(DB_{Tree\ i})) \tag{4}$$

20 The leaf area index (LAI) of each CryoGrid 10x10 m grid cell in LAVESI is then the sum of leaf area values of present trees. When a tree crown area covers more than one cell, the value is distance-weighted on the closest grid cells. For each species, the crown radius is estimated from field data with a log-log linear regression and the slope and y-intercept are used in LAVESI, parameters *crownradiusestslope* and *crownradiusestinterc*, respectively (Table 1).

2.1.4 Addition of a dynamic litter layer and estimating active-layer thickness (ALT)

25 A dynamic, growing litter layer with constant growth of 0.5 cm yr⁻¹ and stochastic disturbance effects was introduced in the *Environmentupdate*-function of LAVESI. When the parameter "*litterlayer*" is switched on, each of the 20 cm grid cells have a chance that the *litterlayerheight* can be reduced. This is stochastically implemented and for each year there is a 10% chance the litter layer is reduced by 10%, a 9% chance of a 25% reduction, a 0.9% chance of 50%, a 0.09% chance of 90%, and a 0.01% chance of a 99% reduction. This leads to a litter layer of ~15 cm in the areas of interest in simulation runs, as is observed

30 in the region of interest (Kruse et al., 2019a). With this functionality, locally acting insulation effects are included in the estimation of the actual ALT in one environment grid cell. The estimation of the maximum active-layer thickness was already

introduced in the original setup of LAVESI (Kruse et al., 2016) and still serves as a first estimate thus making it possible to run a stand-alone simulation of LAVESI without coupling to the CryoGrid (see below).

2.1.5 Parameterization and validation

We compared results from simulations until year 2015 with field inventories from the 2018 expedition, focusing on the following key regions: Lake Khamra (westernmost, warmest), Nyurba (intermediate, climate station), and Spasskaya Pad (easternmost for boreal forests of Yakutia) for which we used literature values for comparison. Values were in the range of expected results.

2.2 The 1D permafrost model CryoGrid

2.2.1 Description and updates

The model used to simulate the thermo-hydrological interactions between permafrost ground and the forest canopy is based on CryoGrid (originally described in Westermann et al. 2016). CryoGrid is a one-dimensional, numerical land surface model that simulates the thermo-hydrological regime of permafrost ground by numerically solving the heat-conduction equation. The CryoGrid model has recently been extended by a multilayer canopy module developed by Bonan et al. (2014) for use in boreal permafrost regions (see Stuenzi et al. 2021a and 2021b for model details). The multilayer canopy model provides a comprehensive parameterization of fluxes from the ground, through the canopy layer up to a roughness sublayer. In combination with CryoGrid the canopy model replaces the standard surface energy balance scheme while soil state variables are passed back to the forest module. Following Stuenzi et al. (2021b), a realistic canopy structure is simulated by allowing fractional compositions of deciduous and evergreen taxa within a simulated forest stand.

This entire model setup has previously been extensively validated for different study sites throughout our study region, including Nyurba (63.08°N, 117.99°E), Spasskaya (62.14°N, 129.37°E), and Ilirney (67.40°N, 168.37°E) (Stuenzi et al. 2021a and 2021b). Validation exercises were carried out based on measured and modelled ground surface temperature (GST), active-layer thickness (ALT), soil moisture, bowen ratio, and short- and longwave radiation below and above the canopy. Parameters defining the canopy, snow, and soil properties were set according to literature values, model documentation, and own measurements (see Stuenzi et al. 2021b for constants and multilayer canopy parameter choices). Table 2 summarizes the parameter choices for the three different sites. Table C1 summarizes the commonly used CryoGrid parameters.

2.3 Coupling the models

The coupled model set-up benefits from the detailed process implementation gained while developing the individual models and brings the 1D to a landscape simulation. Therefore, we can reproduce the energy transfer and thermal regime in permafrost ground as well as the radiation budget, nitrogen and photosynthetic profiles, canopy turbulence, and leaf fluxes, while at the

same time predicting the expected establishment, die-off, and treeline movements of larch forests (Fig. 2). In our analyses, we focus on vegetation and permafrost dynamics and reveal the magnitudes of different feedback processes between permafrost, vegetation, and current and future climate in Siberia.

5   LAVESI serves as host model and can now be set to call individual CryoGrid instances in a given year. For this, the data in LAVESI are aggregated on a 10x10 m grid superimposed on the 20x20 cm grid. Key state variables are leaf area index (LAI), plant area index (PAI), fraction of deciduous species, litter layer height, organic layer height, albedo, and the soil humidity in percent (= plant available water, PAW), which are provided to CryoGrid. These values can either be sorted by LAI and exported for 5 quartiles (implemented but not used here) or from the three areas that are equal slices from left to right (used here, see
10   Appendix A1-A3). When the output file is created, LAVESI can be set to either start CryoGrid directly via a system call or scheduling the instance with a bash file for the workload manager slurm (Yoo et al., 2003). Based on the key state variables provided by LAVESI for each of the areas, CryoGrid starts three (or five) parallel simulations. Once the output has been written, LAVESI reads the file and produces for the three levels anomalies for available soil water and active-layer thickness. With these anomalies, the 10x10 m CryoGrid-grid in LAVESI is filled and from this, the anomalies used to calculate the new
15   values for each 20x20 cm environment grid cell. When the quartile-mode is set, the state values are assigned to this grid calculated by linear interpolation of the LAI-sorted state values and anomalies are calculated as in the other mode.

The multilayer canopy model in CryoGrid requires a minimum LAI of 0.7 m^2 m^{-2} and a minimum height of 1 m to successfully build the radiative transfer scheme from the atmosphere to the ground, therefore forest covers below these values are ignored.

2.4 Forcing data and landscape of focus areas

20   The meteorological forcing data required by the multilayer canopy-permafrost model (air temperature, air pressure, wind speed, relative humidity, solid and liquid precipitation, incoming long- and shortwave radiation, and cloud cover) are obtained from ERA-5 (ECMWF Reanalysis, Hersbach et al., 2018) extracted for the study sites (Nyurba 63.08°N, 117.99°E covering sites EN18067,-68,-70, Spasskaya Pad 62.14°N, 129.37°E, and Lake Khamra 59.97°N, 112.96°E covering EN18079–83, Fig. 1).

25   To provide a millennia-long time series for model spin-up of LAVESI these series were matched to historical climate data for the forcing retrieved from the 0.5°x0.5° Climate Research Unit gridded Time Series (CRU TS version 3.23) monthly data (1901–2014) (Harris et al., 2020). By repeating the 20th century data in a loop, a 2100-year long monthly climate series was established from 1 to 2100 CE for each focus region using the RCP 2.6 prediction scenario.

2.5 Simulation experiments

30   We forced LAVESI simulations with the RCP 2.6 climate scenario calling CryoGrid first in 2015 and yearly in the following years, letting the simulation run until the year 2030. Simulation runs were started with the updated LAVESI version on an empty landscape with true topography starting at 1 CE to allow for spin up and ending in 2100 CE. Into the empty landscape,

seeds (5000 ha^{-1} yr^{-1}) for initiating population establishment were introduced for the first 50 years. Subsequently, only 100 ha^{-1} yr^{-1} seeds were introduced to allow for re-establishment after a complete die-out of trees on the whole simulation area. Each simulation was rerun without calling CryoGrid to compare the differences when the improved active-layer thickness and available soil water is used.

5   In addition to the simulation that uses equal proportions of seeds of each species introduced into the simulation area, we started individual simulations for each single species.

2.6 Statistical analyses

All statistical analyses in this study were performed in R 3.6.1 (R Core Team, 2019), mostly using included standard functions, with the addition of functions from the package "lattice" (Sarkar, 2008) for plotting the data.

10   **3 Results**

3.1 Comparing simulations with LAVESI and the coupled version

The values are very similar for the runs with all and individual species. In nearly all years, LAVESI overestimates ALT by up to 20 cm (mean over all is 109.6±11.4 cm versus 96.1±10.2 cm, which is ~14.1%) at all focus regions (Fig. 3). The soil humidity anomaly fluctuates around 0% at Lake Khamra, is overestimated for Nyurba by ~10%, and Spasskaya Pad by ~20%

15   (Fig. 4). Both are corrected in the coupled version of LAVESI-CryoGrid.

A gradient of LAI forms, which follows the TWI gradient on all sites (I: left, driest to III: right, wettest, Fig. 5 & 6 & 7). Further, a LAI gradient from Khamra (southwest, warmest) via Nyurba (intermediate) to Spasskaya Pad (northeast, coldest) falls together with an increase of larch dominance towards nearly pure larch tree stands. Regarding other species, PISY is

20   present in mixed stands in small numbers and grows only in open stands in simulations with only this species, suggesting that this species prefers a certain environment (Appendix A & D). PIOB performs better in single mono-specific runs leading to larger LAI than in mixed stands, but also reaches dense populations in warm areas (Khamra) and has smallest sizes at coldest sites (Spasskaya Pad, Fig. 5 & 6 & 7). LAGM grows under most conditions but not in the wettest areas (highest TWI values, Appendix D).

A drop in LAI values can be observed in all simulations when LAVESI is updated by CryoGrid (comparing lower to upper panels in Fig. 5 & 6 & 7). In CryoGrid coupled runs, species grow with less dense stands but still cover the same area. In the coupled runs, populations die out in some cases at the end of the simulation at year 2030 (Appendix D).

4 Discussion

The simulations using site information for the three focus sites yield dense tree stands in LAVESI simulations but not in the coupled version. The coupled model results in smaller key soil parameters, active-layer thickness (ALT), and plant available water (PAW). PAW has a strong impact as trees grow poorly in conditions exceeding drought and waterlogging thresholds
5 (e.g. Liang et al., 2014, Mamet et al., 2019, Lawrence et al., 2015, Barber et al., 2000). Drought leads to a higher mortality of trees and in consequence, population simulations are driven close to extinction within the simulation duration of 15 years. However, when drought-adapted *Pinus sylvestris* occupies the niche, there is nearly no change and it could, in the end, colonize the simulation areas. This implies that the model is reproducing the natural dynamics well.

10 Species preference matches observations and expectations (Kuznetsova et al., 2010). Larches have a wide ecological niche and are widespread (Mamet et al., 2019). They are generalists and best adapted to the harsh Siberian environments that were predominantly wet but are now become drier with global warming. *Picea obovata* grows best in the westernmost, warm areas and reaches larger LAI/biomass than when growing in mixed stands competing with other species. This could be attributed to (intraspecific) competition, which, as Wieczorek et al. (2017) shows, seems to be a strong factor dampening the response of
15 tree stands when climatic conditions improve.

As fires become more intense and frequent under global warming, spruce or other species may become dominant rather than shade-intolerant larch species. In the currently naturally deciduous, larch covered areas, evergreen taxa may invade and change the heat fluxes and energy balance with the threat of entering a positive feedback loop such as a deepening of the ALT (Bonan,
20 2008, Stocker et al., 2013, Stuenzi et al., 2021b).

In general, technical issues arise when coupling models and implementing I/O indirectly via output files. The two different time-steps (years in LAVESI vs. 5 minutes in CryoGrid) and computational speeds lead to long computation times and high requirements of computational resources of the coupled version. To avoid any delay, a parallelization of CryoGrid simulations,
25 as implemented here, is highly recommended, especially for dry study sites where a simulated year in CryoGrid can take up to 4 hours. We find that simulations of homogeneous areas perform best and especially that the exchange is set up using three to five instances sorted by LAI. The constraint lies here and more instances would improve the representation of variants of deciduous/evergreen covered plots but these improved LAVESI simulations come at the cost of computation time when not using the parallelized version as developed for this study.

30 ## 5 Conclusions

The as-is application of LAVESI overestimates ALT values by around 14% therefore we advise using the implemented correction from CryoGrid for forecasting forest dynamics in the proposed coupled version. The 3D simulations provide a way

to understand permafrost distribution and interactions with vegetation. Further implementations, tracked online in the github repository of LAVESI, include spatially explicit fire and trait variation and adaptation. This public sharing of the source code plus advances in both models allows the easy exchange, development, and adaptation to further regions. This and the simple set-up make the coupled model version easy to implement and thus offers a wide applicability. However, fieldwork or literature

5   values from remote areas are necessary to adjust parameters and adapt the model and species to local site conditions, which is an issue for the vast remote areas in Siberia. With increasing data from these remote areas, such as better satellite imagery coverage and resolution, the collection of more detailed field data (loggers recording soil temperatures and moisture in the active layer), and monitoring of permafrost dynamics and tree growth, the drivers of forest dynamics may be disentangled and thus improve the model.

6 Acknowledgements

We are grateful for the support of Sven N Willner in parallelizing LAVESI. The data and experience gained on the successful Expedition Chukotka and Central Yakutia in 2018 was the basis for the developments and we thank especially Luidmila A Pestryakova for her support and leadership of the expedition, but all participants involved in the expedition. We thank Luca Farcas and Christopher Guth for their support in preparing samples and establishing tree-ring chronologies, and Ingo Heinrich

15   from the GFZ dendro lab for their support of the dendroecological analyses. We thank Iuliia Shevtsova for supporting the organization and analyses of the biomass data. We thank especially the HPC support at AWI mainly Natalya Rakowski and Malte Thoma for their assistant in the simulation setup.

This study has been supported by the ERC consolidator grant Glacial Legacy to Ulrike Herzschuh (no. 772852). Further, the work was supported by the Federal Ministry of Education and Research (BMBF) of Germany through a grant to Moritz Langer

20   (no. 01LN1709A). Funding was additionally provided by the Helmholtz Association in the framework of MOSES (Modular Observation Solutions for Earth Systems).

7 Data availability

The CryoGrid code is available on Zenodo (https://doi.org/10.5281/zenodo.5119987). LAVESI is publicly available on GitHub at   https://github.com/StefanKruse/LAVESI   the   branch   used   for   this   study   is

25   https://github.com/StefanKruse/LAVESI/tree/CryoGrid_multispecies and the commit used for the simulations for this study is 93a9767 and the final commit will be permanently stored on Zenodo upon acceptance of the manuscript.

Biomass data and tree-ring growth information for the species present at the ROI is available upon request and will be stored publicly upon acceptance of the manuscript to PANGAEA https://www.pangaea.de/

Author contributions

Stefan Kruse SK and Ulrike Herzschuh UH developed the idea of coupling LAVESI with CryoGrid. SK and Simone Stuenzi SMS set up the coupled version and maintained the simulation runs together. Josias Gloy JG developed the upgrade to implement multiple species efficiently in LAVESI, SK realized the implementation of the LAVESI related programming. SK
5   analysed the data and drafted the first version of the manuscript, which was jointly edited by all authors.

The authors declare no conflict of interest.

References

Abaimov, A. P., Lesinski, J. A., Martinsson, O., and Milyutin, L. I.: Variability and Ecology of Siberian Larch Species.
10   Swedish Univ. of Agricultural Sciences, Umeå (Sweden). Dept. of Silviculture, 75, 1998.

Barber, V.A., Juday, G.P., & Finney, B.P.: Reduced growth of Alaskan white spruce in the twentieth century from temperature-induced drought stress. Nature 405, 668–673, https://doi.org/10.1038/35015049, 2000.

Berner, L. T., Beck, P. S. A, Bunn, A. G., and Goetz, S. J.: Plant response to climate change along the forest-tundra ecotone in northeastern Siberia. Glob Change Biol, 19, 3449–3462. https://doi.org/10.1111/gcb.12304, 2013.

15   Biskaborn, B. K., Brieger, F., Herzschuh, U., Kruse, S., Pestryakova, L., Shevtsova, I., Stuenzi, S., Vyse, S., and Zakharov, E.: Glacial lake coring and treeline forest analyses at the northeastern treeline extension in Chukotka. In S. Kruse, D. Bolshiyanov, M. N. Grigoriev, A. Morgenstern, L. Pestryakova, L. Tsibizov, & A. Udke (Eds.), Russian-German Cooperation: Expeditions to Siberia in 2018. Berichte zur Polar-und Meeresforschung [Reports on polar and marine research] (Vol. 734, pp. 139–147). Bremerhaven: Alfred Wegener Institute for Polar and Marine Research.
20   https://doi.org/10.2312/BzPM_0734_2019, 2019.

Błasiak, A., Węgiel, A., Łukowski, A., Sułkowski, S., and Turski, M. : The effects of tree and stand traits on the specific leaf area in managed scots pine forests of different ages. Forests, 12. https://doi.org/10.3390/f12040396, 2021.

Boike, J., Nitzbon, J., Anders, K., Grigoriev, M., Bolshiyanov, D., Langer, M., Lange, S., Bornemann, N., Morgenstern, A., Schreiber, P., Wille, C., Chadburn, S., Gouttevin, I., Burke, E., and Kutzbach, L. : A 16-year record (2002–2017) of
25   permafrost, active-layer, and meteorological conditions at the Samoylov Island Arctic permafrost research site, Lena River delta, northern Siberia: an opportunity to validate remote-sensing data and land surface, snow, and permafrost models. Earth Syst Sci Data, 11, 261–299. https://doi.org/10.5194/essd-11-261-2019, 2019.

Bonan, G. B.: Forests and Climate Change: Forcings, Feedbacks, and the Climate Benefits of Forests. Science, 320, 1444–1449. https://doi.org/10.1126/science.1155121, 2008.

30   Bonan, G. B., Williams, M., Fisher, R. A., and Oleson, K. W.: Modeling stomatal conductance in the earth system: Linking leaf water-use efficiency and water transport along the soil–plant–atmosphere continuum. Geosci Model Dev, 7, 2193–2222, https://doi.org/10.5194/gmd-7-2193-2014, 2014.

Bunn, A., Korpela, M., Biondi, F. Campelo, F., Mérian, P., Qeadan, F., and Zang, C.: dplR: Dendrochronology Program Library in R. R package version 1.7.1., https://CRAN.R-project.org/package=dplR, 2020.

Conrad, O., Bechtel, B., Bock, M., Dietrich, H., Fischer, E., Gerlitz, L., Wehberg, J., Wichmann, V., and Böhner, J.: System for Automated Geoscientific Analyses (SAGA) v. 2.1.4. Geosci Model Dev, 8, 1991–2007. https://doi.org/10.5194/gmd-8-1991-2015, 2015.

DeAngelis, D.L. and Mooij, W.M.: Individual-based modeling of ecological and evolutionary processes. Annu. Rev. Ecol. Evol. Syst. 36, 147–168, https://doi.org/10.1146/annurev.ecolsys.36.102003.152644, 2005.

Gorelick, N., Hancher, M., Dixon, M., Ilyushchenko, S., Thau, D., and Moore, R.: Google Earth Engine: Planetary-scale geospatial analysis for everyone. Remote Sens Environ, 202, 18–27. https://doi.org/10.1016/j.rse.2017.06.031, 2017.

Grimm, V. and Railsback, S.F.: Individual-based Modeling and Ecology. Princeton University Press, Princeton, NJ, 2005

Harris, I., Osborn, T. J., Jones, P., and Lister, D.: Version 4 of the CRU TS monthly high-resolution gridded multivariate climate dataset. Sci Data, 7(1), 1–18. https://doi.org/10.1038/s41597-020-0453-3, 2020.

Hersbach, H., Bell, B., Berrisford, P., et al.: The ERA5 global reanalysis. Q J R Meteorol Soc, 146, 1999-2049, https://doi.org/10.1002/qj.3803, 2020.

Herzschuh, U.: Legacy of the Last Glacial on the present-day distribution of deciduous versus evergreen boreal forests. Global Ecol Biogeogr, 29, 198–206. https://doi.org/10.1111/geb.13018, 2020.

Herzschuh, U., Birks, H. J. B., Laepple, T., Andreev, A., Melles, M., and Brigham-Grette, J.: Glacial legacies on interglacial vegetation at the Pliocene-Pleistocene transition in NE Asia. Nat Commun, 7, 1–11. https://doi.org/10.1038/ncomms11967, 2016.

Hijmans, R. J.: raster: Geographic Data Analysis and Modeling. R package version 3.0-12. https://CRAN.R-project.org/package=raster, 2020.

Kirpotin, S. N., Callaghan, T. V., Peregon, A. M., Babenko, A. S., Berman, D. I., Bulakhova, N. A., Byzaakay, Arysia A. Chernykh, T. M., Chursin, V., Interesova, E. A., Gureev, S. P., Kerchev, I. A., Kharuk, V. I., Khovalyg, A. O., Kolpashchikov, L. A., Krivets, S. A., Kvasnikova, Z. N., Kuzhevskaia, I. V., Merzlyakov, O. E., Nekhoroshev, O. G., Popkov, V. K., Pyak, A. I., Valevich, T. O., Volkov, I. V. Volkova, I. I.: Impacts of environmental change on biodiversity and vegetation dynamics in Siberia. Ambio. https://doi.org/10.1007/s13280-021-01570-6, 2021.

Konôpková, A., Vedernikov, K. E., Zagrebin, E. A., Islamova, N. A., Grigoriev, R. A., Húdoková, H., Petek, A, Kmeť, J., Petrík, P., Pashkova, A. S., Zhuravleva, A. N., and Bukharina, I. L.: Impact of the European bark beetle *Ips typographus* on biochemical and growth properties of wood and needles in Siberian spruce *Picea obovata*. Central European Forestry Journal, 66, 243–254. https://doi.org/10.2478/forj-2020-0025, 2020.

Krieger, G., Moreira, A., Fiedler, H., Hajnsek, I., Werner, M., Younis, M., and Zink, M.: TanDEM-X: A satellite formation for high-resolution SAR interferometry. IEEE T Geosci Remote, 45, 3317–3340. https://doi.org/10.1109/TGRS.2007.900693, 2007.

Kruse, S., Wieczorek, M., Jeltsch, F., and Herzschuh, U.: Treeline dynamics in Siberia under changing climates as inferred from an individual-based model for *Larix*. Ecol Model, 338, 101–121. https://doi.org/10.1016/j.ecolmodel.2016.08.003, 2016.

Kruse, S., Epp, L. S., Wieczorek, M., Pestryakova, L. A., Stoof-Leichsenring, K. R., and Herzschuh, U.: High gene flow and
5   complex treeline dynamics of *Larix* Mill. stands on the Taymyr Peninsula (north-central Siberia) revealed by nuclear microsatellites. Tree Genet Genomes, 14, 19, 1–13. https://doi.org/10.1007/s11295-018-1235-3, 2018a.

Kruse, S., Gerdes, A., Kath, N. J., and Herzschuh, U.: Implementing spatially explicit wind-driven seed and pollen dispersal in the individual-based larch simulation model: LAVESI-WIND 1.0. Geosci Model Dev, 11, 4451–4467. https://doi.org/10.5194/gmd-11-4451-2018, 2018b.

10   Kruse, S., Herzschuh, U., Stünzi, S., Vyse, S., and Zakharov, E.: Sampling mixed-species boreal forests affected by disturbances and mountain lake and alas lake coring in Central Yakutia. In S. Kruse, D. Bolshiyanov, M. N. Grigoriev, A. Morgenstern, L. Pestryakova, L. Tsibizov, & A. Udke (Eds.), Russian-German Cooperation: Expeditions to Siberia in 2018. Berichte zur Polar-und Meeresforschung [Reports on polar and marine research] (pp. 148–153). Bremerhaven: Alfred Wegener Institute for Polar and Marine Research. https://doi.org/10.2312/BzPM_0734_2019, 2019a.

15   Kruse, S., Gerdes, A., Kath, N. J., Epp, L. S., Stoof-Leichsenring, K. R., Pestryakova, L. A., and Herzschuh, U.: Dispersal distances and migration rates at the arctic treeline in Siberia – a genetic and simulation-based study. Biogeosciences, 16, 1211–1224. https://doi.org/10.5194/bg-16-1211-2019, 2019b.

Kruse, S., Kolmogorov, A. I., Pestryakova, L. A., and Herzschuh, U.: Long-lived larch clones may conserve adaptations that could restrict treeline migration in northern Siberia. Ecol Evol, 10, 10017–10030. https://doi.org/10.1002/ece3.6660, 2020.

20   Kuznetsova, L. V., Zakharova, V. I., Sosina, N. K., Nikolin, E. G., Ivanova, E. I., Sofronova, E. V., Poryadina, L, N., Mikhalyova, L. G., Vasilyeva, I. I., Remigailo, P. A., Gabyshev, V. A., Ivanova, A. P., and Kopyrina, L. I.: Flora of Yakutia: Composition and Ecological Structure. In E. I. Troeva, A. P. Isaev, M. M. Cherosov, & N. S. Karpov (Eds.), The Far North: Plant Biodiversity and Ecology of Yakutia (Vol. 3, pp. 357–369). Dordrecht, Netherlands: Springer. https://doi.org/10.1007/978-90-481-3774-9, 2010.

25   Langer, M., Westermann, S., Muster, S., Piel, K., & Boike, J.: The surface energy balance of a polygonal tundra site in northern Siberia - Part 1: Spring to fall. Cryosphere, 5, 151–171. https://doi.org/10.5194/tc-5-509-2011, 2011.

Lawrence, D. M., Koven, C. D., Swenson, S. C., Riley, W. J., and Slater, A. G.: Permafrost thaw and resulting soil moisture changes regulate projected high-latitude CO_2 and CH_4 emissions. Environ. Res. Lett. 10, 94011 https://doi.org/10.1088/1748-9326/10/9/094011, 2015.

30   Lehsten, V., Mischurow, M., Lindström, E., Lehsten, D., and Lischke, H.: LPJ-GM 1.0: simulating migration efficiently in a dynamic vegetation model. Geosci Model Dev, 12, 893–908. https://doi.org/10.5194/gmd-12-893-2019, 2019.

Liang, M., Sugimoto, A., Tei, S., Bragin, I. V., Takano, S., Morozumi, T., Shingubara, R., Maximov, T. C., Kiyashko, S. I. Velivetskaya, T. A., and Ignatiev, A. V.: Importance of soil moisture and N availability to larch growth and distribution in

the Arctic taiga-tundra boundary ecosystem, northeastern Siberia. Polar Sci, 8, 327–341. https://doi.org/10.1016/j.polar.2014.07.008, 2014.

MacDonald, G. M., Kremenetski, K. V., and Beilman, D. W.: Climate change and the northern Russian treeline zone. Philosophical Transactions of the Royal Society B: Biological Sciences, 363, 2283–2299. https://doi.org/10.1098/rstb.2007.2200, 2008.

Mamet, S. D., Brown, C. D., Trant, A. J., and Laroque, C. P.: Shifting global *Larix* distributions: Northern expansion and southern retraction as species respond to changing climate. J Biogeogr, 46, 30–44. https://doi.org/10.1111/jbi.13465, 2019.

Mencuccini, M. and Bonosi, L.: Leaf/sapwood area ratios in Scots pine show acclimation across Europe. Can J Forest Res, 31, 442–456. https://doi.org/10.1139/cjfr-31-3-442, 2001.

Nitzbon, J., Langer, M., Westermann, S., Martin, L., Aas, K. S., and Boike, J.: Pathways of ice-wedge degradation in polygonal tundra under different hydrological conditions. Cryosphere, 13, 1089–1123. https://doi.org/10.5194/tc-13-1089-2019, 2019.

Pinheiro, J., Bates, D., DebRoy, S., and Sarkar, D.: nlme: Linear and Nonlinear Mixed Effects Models. R package version 3.1-140, https://CRAN.R-project.org/package=nlme, 2019.

R Core Team: R: A Language and Environment for Statistical Computing. Vienna, Austria. Retrieved from https://www.r-project.org/, 2019.

Rees, W. G., Hofgaard, A., Boudreau, S., Cairns, D. M., Harper, K., Mamet, S., Mathisen, I., Swirad, Z, and Tutubalina, O.: Is subarctic forest advance able to keep pace with climate change? Glob Change Biol, 26, 3965–3977. https://doi.org/10.1111/gcb.15113, 2020.

Reich, P. B., Walters, M. B., Ellsworth, D. S., Vose, J. M., Voliin, J. C., Gresham, C., and Bowman, W. D.: Relationships of leaf dark respiration to leaf nitrogen, specific leaf area and leaf life-span: a test across biomes and functional groups. Oecologia. 114, 471-482. https://doi.org/ 10.1007/s004420050471, 1998.

Sarkar, D.: Lattice: Multivariate Data Visualization with R. Springer, New York. ISBN 978-0-387-75968-5, 2008.

Sato, H., Kobayashi, H., Iwahana, G., and Ohta, T.: Endurance of larch forest ecosystems in eastern Siberia under warming trends, Ecol Evol, 6, 5690–5704, https://doi.org/10.1002/ece3.2285, 2016

Shevtsova, I., Herzschuh, U., Heim, B., Schulte, L., Stünzi, S., Luidmila, A., Zakharov, E. S Kruse, S.: Recent above-ground biomass changes in central Chukotka (Russian Far East) using field sampling and Landsat satellite data. Biogeosciences, 18, 3343–3366. https://doi.org/10.5194/bg-18-3343-2021, 2021.

Snell, R. S.: Simulating long-distance seed dispersal in a dynamic vegetation model. Global Ecol Biogeogr, 23, 89–98. https://doi.org/10.1111/geb.12106, 2014.

Snell, R. S. and Cowling, S. A.: Consideration of dispersal processes and northern refugia can improve our understanding of past plant migration rates in North America. Journal of Biogeography, 42, 1677–1688. https://doi.org/10.1111/jbi.12544, 2015.

Stocker, B. D., Roth, R., Joos, F., Spahni, R., Steinacher, M., Zaehle, S., Bouwman, L., and Prentice, I. C.: Multiple greenhouse-gas feedbacks from the land biosphere under future climate change scenarios. Nat Clim Change, 3, 666–672, https://doi.org/10.1038/nclimate1864, 2013.

Stuenzi, S. M., Boike, J., Cable, W., Herzschuh, U., Kruse, S., Pestryakova, L. A., Schneider von Deimling, T., Westermann S., Zakharov, E. S., and Langer M.: Variability of the surface energy balance in permafrost-underlain boreal forest. Biogeosciences, 18, 343–365. https://doi.org/10.5194/bg-18-343-2021, 2021a.

Stuenzi, S. M., Boike, J., Gädecke, A., Herzschuh, U., Kruse, S., Pestryakova, L. A., Westermann S., and Langer M. (2021b). Variability of the surface energy balance in permafrost-underlain boreal forest. ERL, 16, 084045. https://doi.org/10.1088/1748-9326/ac153d, 2021b.

Westermann, S., Langer, M., Boike, J., Heikenfeld, M., Peter, M., Etzelmüller, B., and Krinner, G.: Simulating the thermal regime and thaw processes of ice-rich permafrost ground with the land-surface model CryoGrid 3, Geosci Model Dev, 9, 523–546. https://doi.org/10.5194/gmd-9-523-2016, 2016.

Wieczorek, M., Kruse, S., Epp, L. S., Kolmogorov, A., Nikolaev, A. N., Heinrich, I., Jeltsch, F., Pestryakova, L. A., Zibulski, R., and Herzschuh, U.: Dissimilar responses of larch stands in northern Siberia to increasing temperatures-a field and simulation based study. Ecology, 98, 2343–2355. https://doi.org/10.1002/ecy.1887, 2017.

Xian-Kui, Q.and Chuan-Kuan, W.: Comparison of foliar water use efficiency among 17 provenances of *Larix gmelinii* in the Mao'ershan area. Chinese Journal of Plant Ecology, 39, 352–361. https://doi.org/10.17521/cjpe.2015.0034, 2015.

Yoo, A. B., Jette, M. A., and Grondona, M.: SLURM: Simple Linux Utility for Resource Management. Lect Notes Comput Sc (including subseries Lecture Notes in Artificial Intelligence and Lecture Notes in Bioinformatics), 2862, 44–60, https://doi.org/10.1007/10968987_3, 2003.

Zhang, W., Miller, P. A., Smith, B., Wania, R., Koenigk, T., and Döscher, R.: Tundra shrubification and tree-line advance amplify Arctic climate warming: results from an individual-based dynamic vegetation model. Environ. Res. Lett. 8, 034023, https://doi.org/10.1088/1748-9326/8/3/034023, 2013.
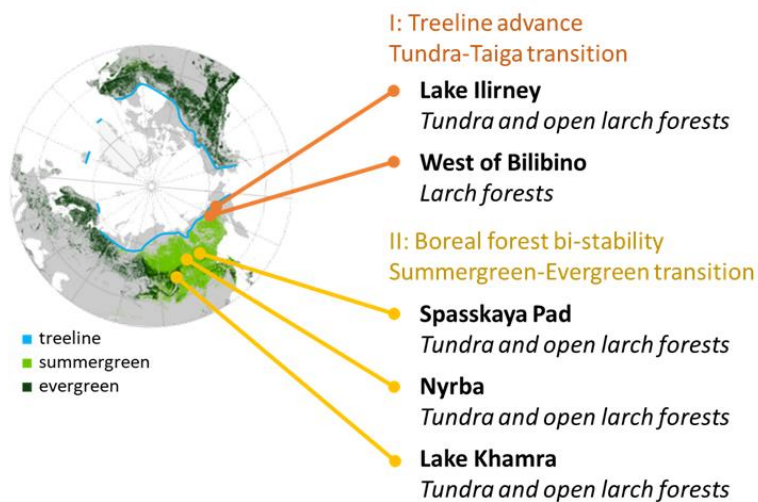
Figure 1: Scheme of focus areas covered on the Chukotka and Central Yakutia 2018 expedition. Region II: Boreal forest bi-stability summergreen-evergreen transition needed for the expansion of species in addition to *Larix cajanderi* and *L. sibirica*.
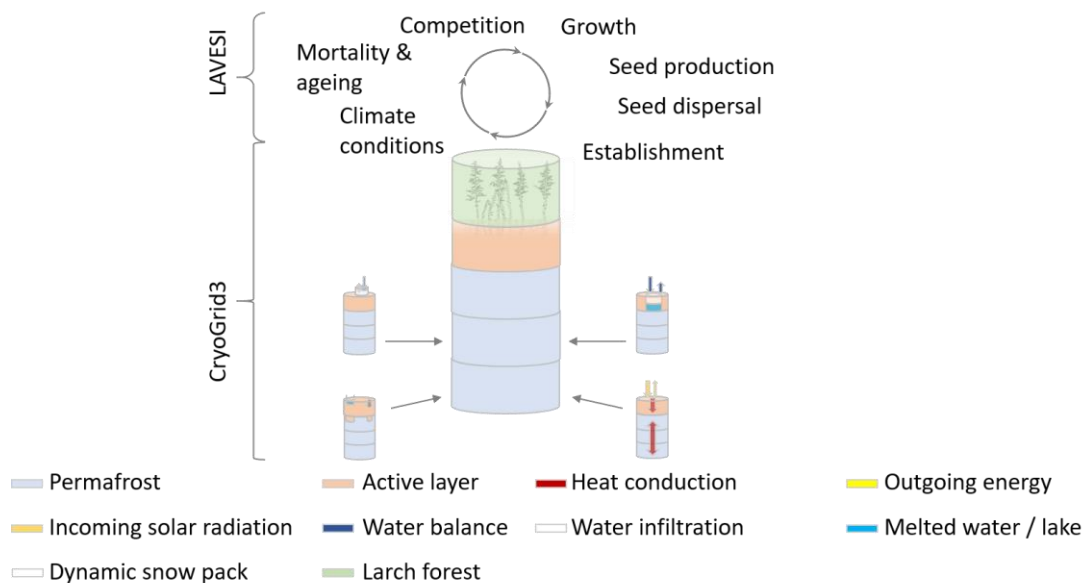
5   **Figure 2: Scheme of coupling CryoGrid and LAVESI and involved processes.**
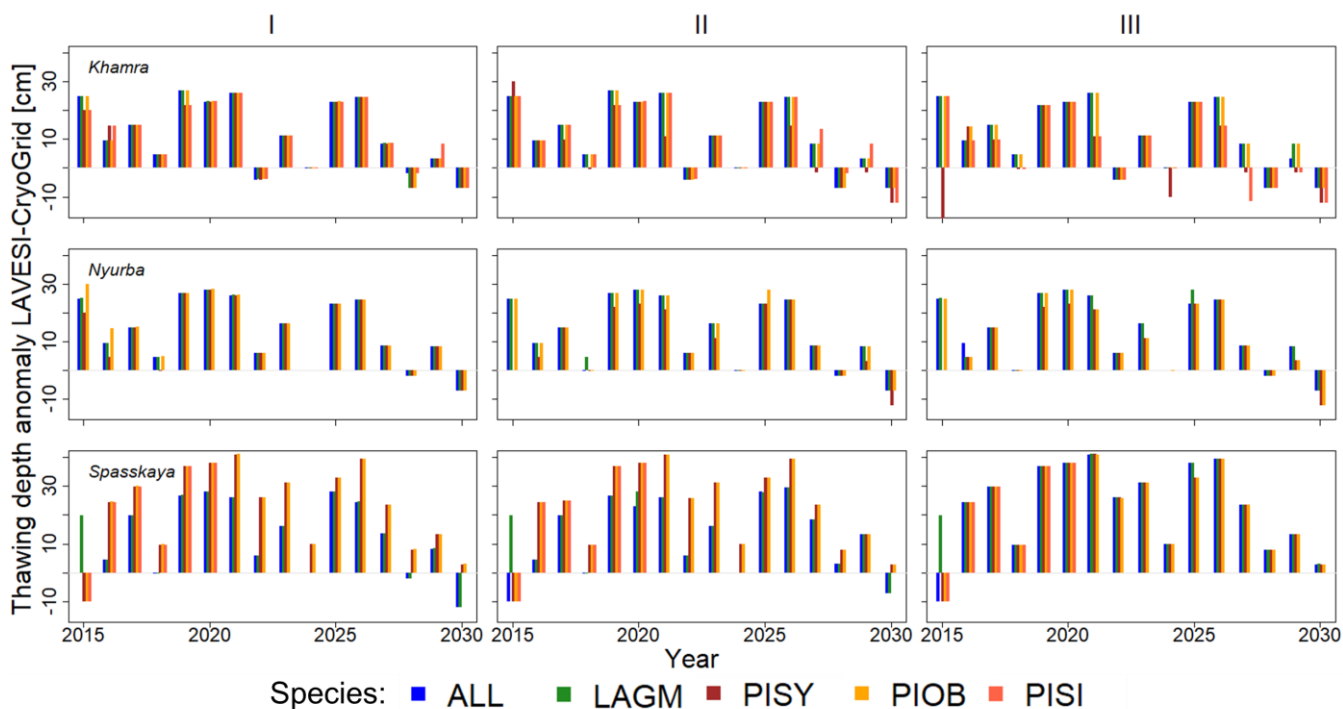
Figure 3. Thawing depth anomaly in the coupled simulation model for all focus areas (rows) and areas within the simulation areas (columns: I, II and III) for year steps 2015-2030. LAGM *Larix gmelinii*; **PIOB** *Picea obovata*; **PISI** *Pinus sibirica*; **PISY** *Pinus sylvestris*.
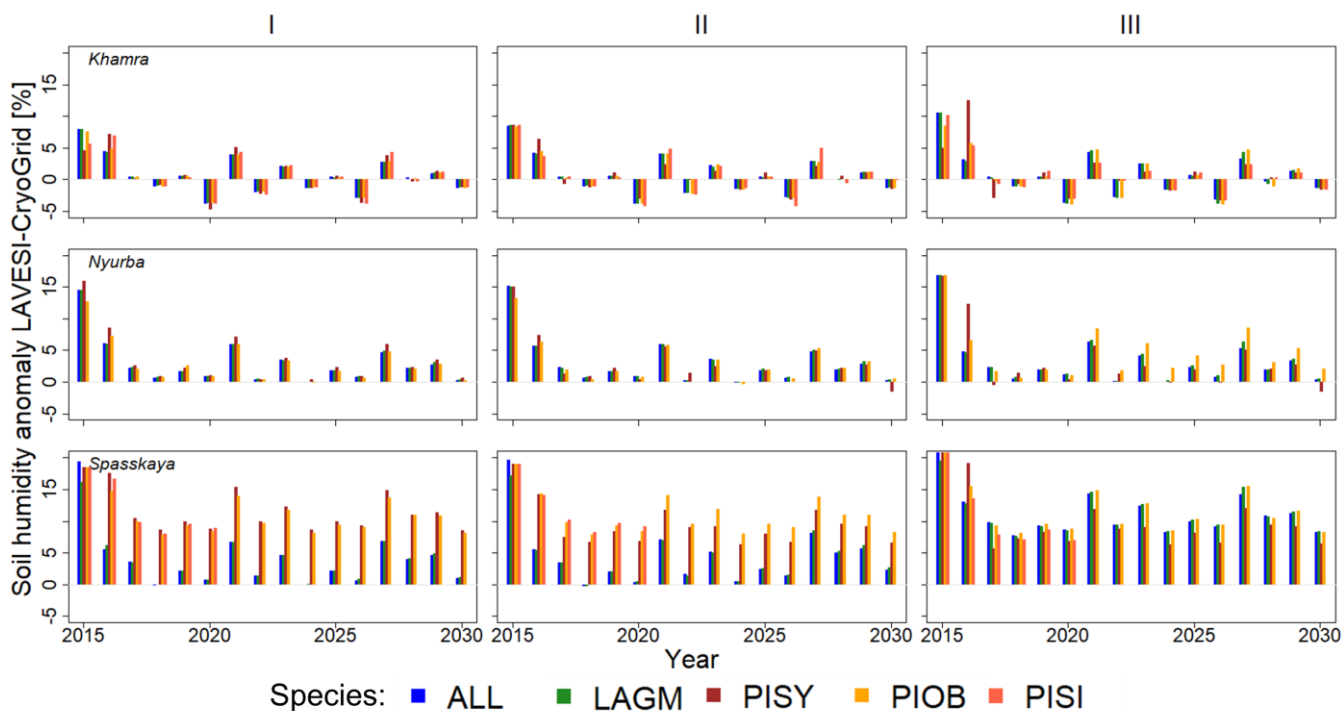
Figure 4. Soil humidity anomalies in the coupled simulation model for all focus areas (rows) and areas within the simulation areas (columns: I, II and III) for year steps 2015-2030. LAGM *Larix gmelinii*; PIOB *Picea obovata*; PISI *Pinus sibirica*; PISY *Pinus sylvestris*.
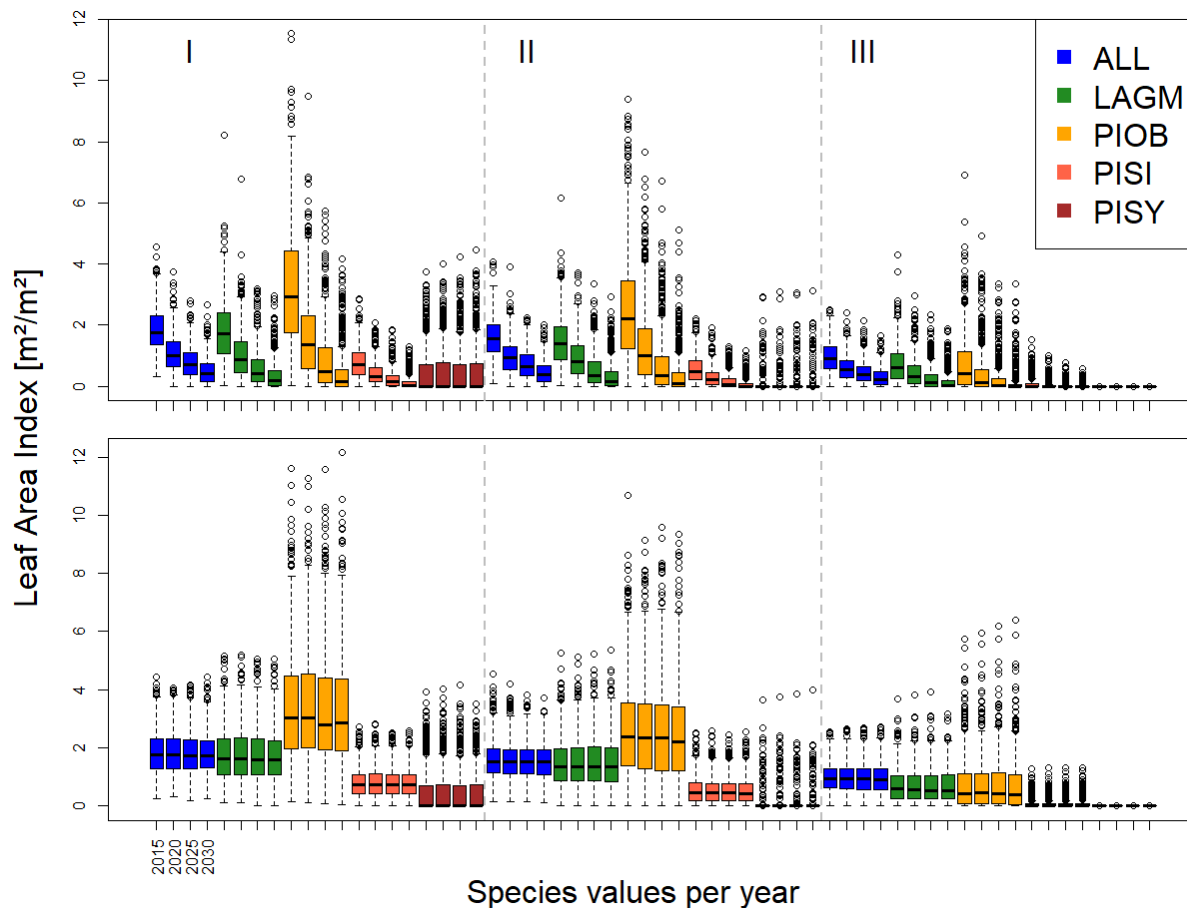
Figure 5. Leaf area index (LAI) values at Lake Khamra for the three areas within the simulation areas (I, II, III) on the same plot at which CryoGrid was called (upper row) and only LAVESI runs (lower row). LAGM *Larix gmelinii*; **PIOB** *Picea obovata*; **PISI** *Pinus sibirica*; **PISY** *Pinus sylvestris*.
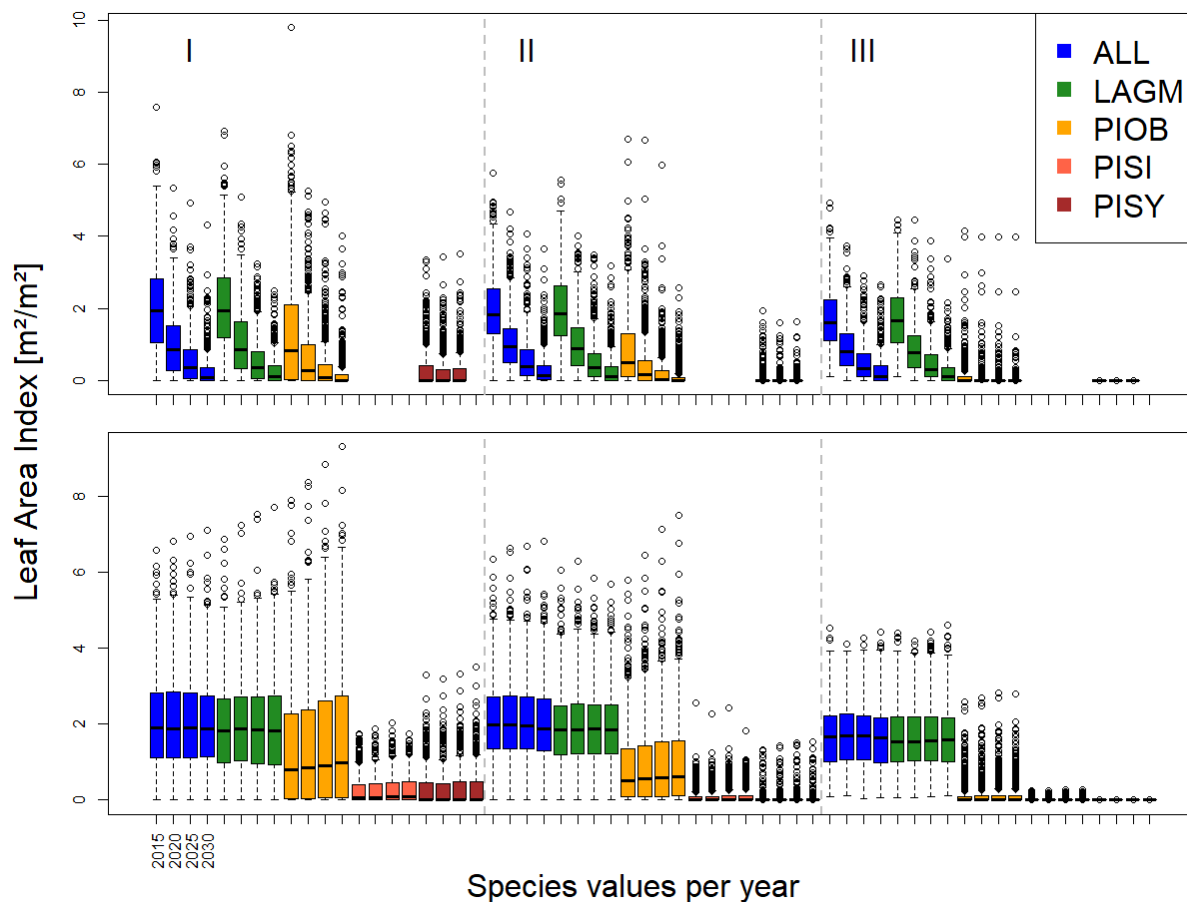
Figure 6. Leaf area index (LAI) values at Nyurba for the three areas within the simulation areas (I, II, III) on the same plot at which CryoGrid was called (upper row) and only LAVESI runs (lower row). LAGM *Larix gmelinii*; PIOB *Picea obovata*; PISI *Pinus sibirica*; PISY *Pinus sylvestris*.
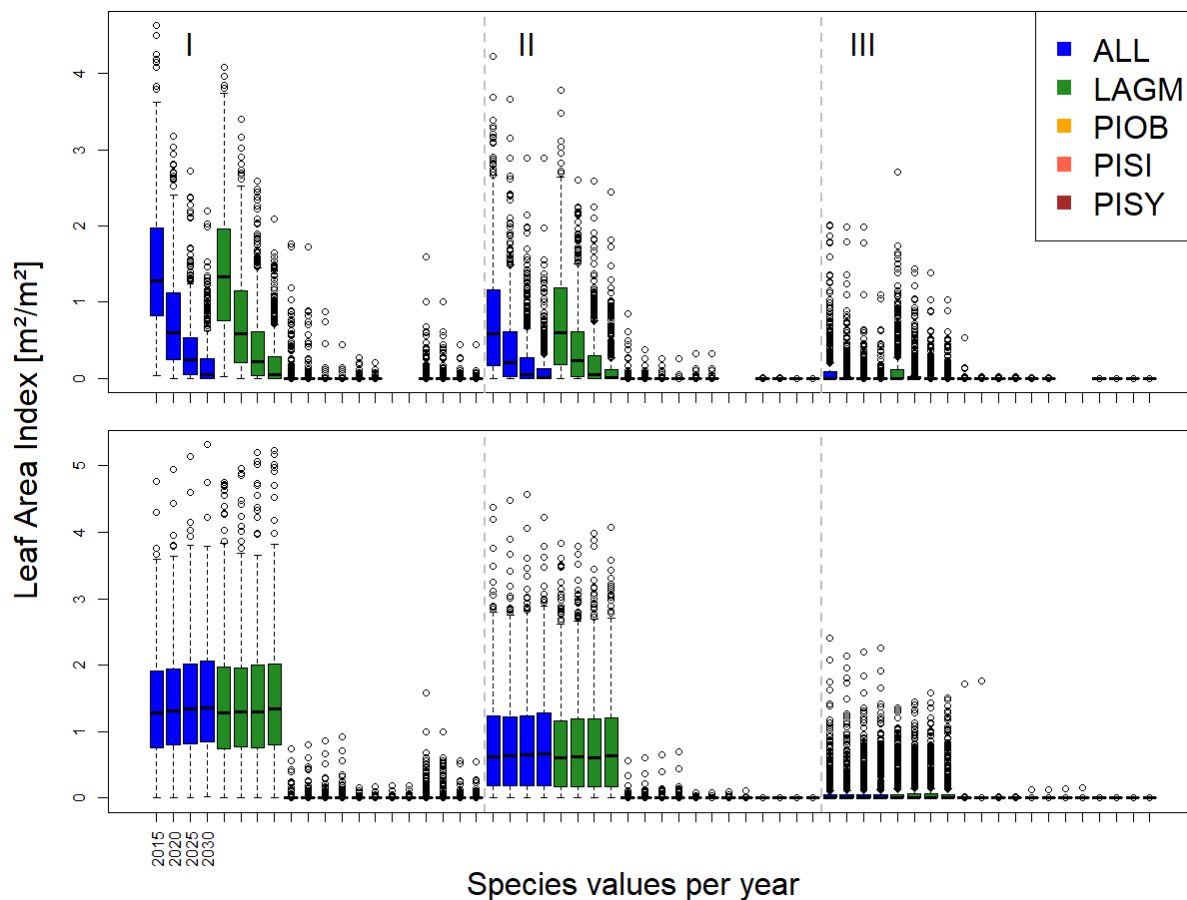
Figure 7. Leaf area index (LAI) values at Spasskaya Pad for the three areas within the simulation areas (I, II, III) on the same plot at which CryoGrid was called (upper row) and only LAVESI runs (lower row). LAGM *Larix gmelinii*; **PIOB** *Picea obovata*; **PISI** *Pinus sibirica*; **PISY** *Pinus sylvestris*.

Table 1. Species traits and variable values in LAVESI newly introduced for this study. References from * Abaimov et al., 1998, or ** Sato et al., 2010, or educated guess.

Parameter		Species					
Description	Abbreviation	*Larix gmelinii*	*Larix sibirica*	*Larix cajanderi*	*Picea obovata*	*Pinus sylvestris*	*Pinus sibirica*
Internal species variable [#]	*Species*	1	2	3	4	5	6
Species abbreviation	-	LAGM	LASI	LACA	PIOB	PISY	PISI
Asymmetry of height estimation model	*Heightloga*	9.415	9.415	9.415	10.827	28.719	11.590869
Centre of height estimation model	*Heightlogb*	2.83	2.83	2.83	3.543	10.939	4.102115
Scaling factor of height estimation model	*Heightlogc*	2.214	2.214	2.214	2.381	4.916	3.057776
Mortality rate of windthrow	*Mwindthrow*	0.01	0.01	0.01	0.01	0.01	0.01
Minimum depth of active layer table [cm]	*minactivelayer*	20*	200	20	200	100	200
Minimum available soil water content [%]	*minsoilwater*	21.1**	10	10	10	10	25
Rooting depth [cm]	*rootingdepth*	50*	100	20	200	100	100
Relative bark thickness value	*relbarkthickness*	2	2	2	1.5	3	3
Chance of resprouting following wildfire	*resprouting*	0.01	0	0.01	0	0	0
Slope of leaf biomass estimation model	*biomassleaffaca*	1.955683	1.955683	2.162319	2.482039	2.260794	2.125194
Slope of woody biomass estimation model	*biomasswoodfaca*	3.553949	3.553949	3.901602	3.844512	3.257366	3.541813
Deciduousness (binary: 1/0, yes/no)	*deciduous*	1	1	1	0	0	0
Slope of crown radius estimation model	*crownradiusestslope*	0.728231	0.728231	0.9193333	0.6007845	0.7899374	0.5785676
Intercept of crown radius estimation model	*crownradiusestinterc*	2.794274	2.794274	2.4618496	2.9118007	2.4135727	2.9459064
Slope of leaf area estimation model	*leafareaslope*	2.017164	2.017164	2.236605	2.242359	2.015382	1.927198

Table 2. Study site parameters for CryoGrid.

Study site	Soil layer depth (Litter/Organic /Mineral)	Respective soil type	ERA-interim coordinate
Nyurba	0/0.07/0.16	Peat/Clay/Sand	N 63.08°, E 117.99°
Spasskaya	0/0.08/0.16	Peat/Clay/Sand	N 62.14°, E 129.37°
Khamra	0/0.05/0.9	Peat/Clay/Sand	N 59.98°, E 112.96°

Appendix

Appendix A. Landscape defining the focus region's plot area.
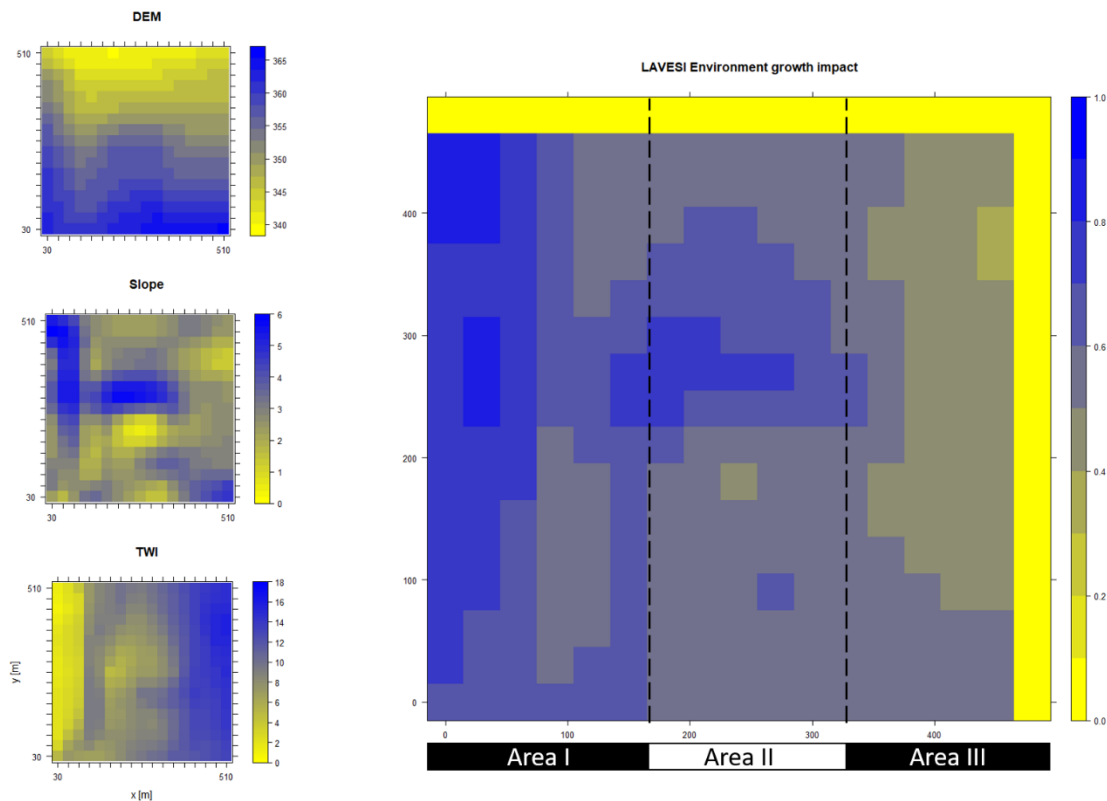
Figure A1. Elevation (DEM), slope angle, and terrain water index (TWI) define the environment growth impact (0 no growth possible; 1 good, no constraints) using an empirically fitted function for present forest growth at area of interest Khamra.
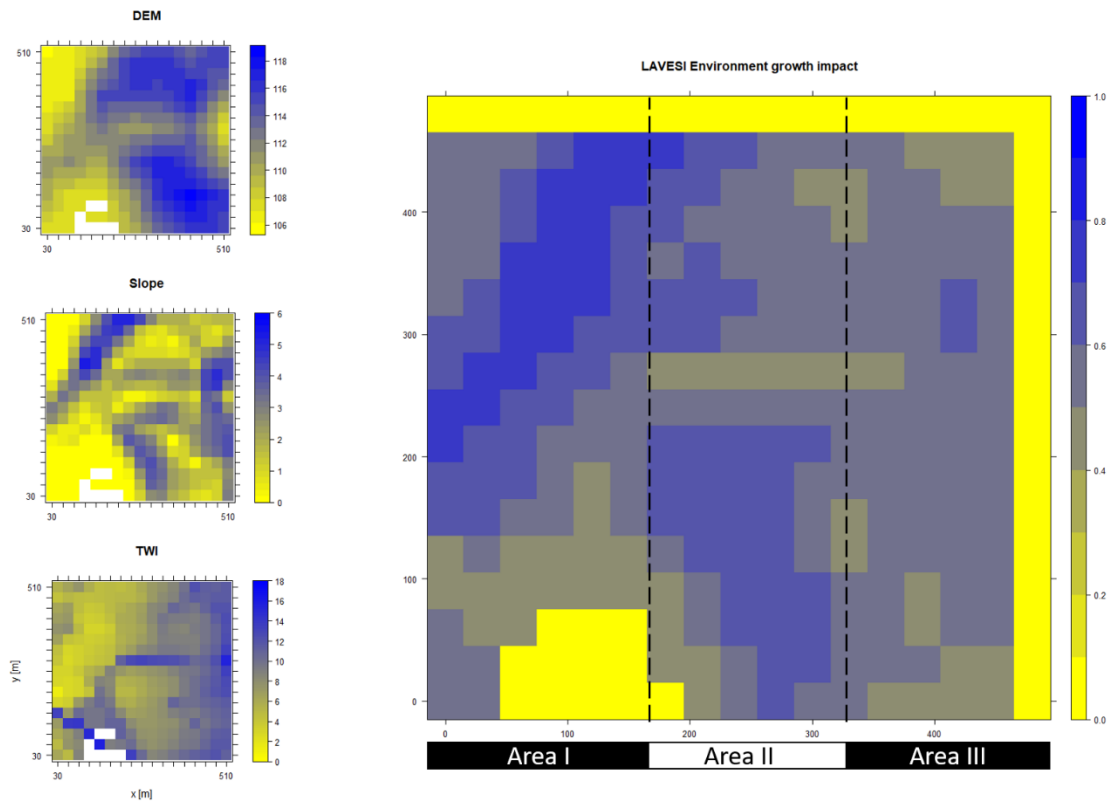
Figure A2. Elevation (DEM), slope angle, and terrain water index (TWI) define the environment growth impact (0 no growth possible; 1 good, no constraints) using an empirically fitted function for present forest growth at area of interest Nyurba.
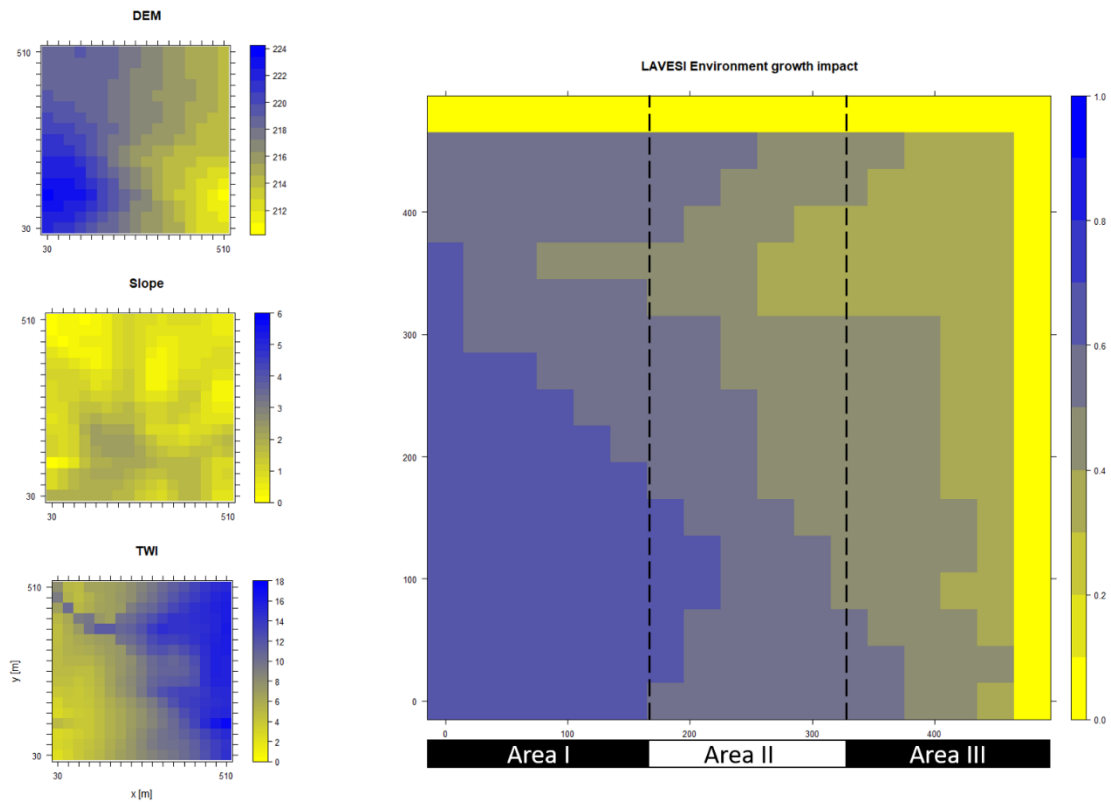
Figure A3. Elevation (DEM), slope angle, and terrain water index (TWI) define the environment growth impact (0 no growth possible; 1 good, no constraints) using an empirically fitted function for present forest growth at area of interest Spasskaya Pad.

Appendix B. LAVESI model parameters and constants used

Table B1. Variable in LAVESI. See Kruse et al., 2016, 2018, and 2019b for a detailed description.

Parameter Description	Abbreviation	Species Larix gmelinii	Larix sibirica	Larix cajanderi	Picea obovata	Pinus sylvestris	Pinus sibirica
Internal species variable [#]		1	2	3	4	5	6
Species abbreviation		LAGM	LASI	LACA	PIOB	PISY	PISI
	coneage	15	15	15	15	15	15
	seedflightrate	0.63931	0.63931	0.63931	0.63931	0.63931	0.95
	seedtravelbreeze	60.1	45	60.1	15	30	30
	seeddescent	0.86	0.93	0.86	1.2	2.4	2.4
	distanceratio	0.16	0.16	0.16	0.16	0.16	0.16
	seedprodfactor	8	8	8	8	8	16
	germinationrate	0.01	0.01	0.01	0.01	0.01	0.01
	germinationweatherinfluence	0.447975	0.447975	0.447975	0.447975	0.447975	0.447975
	gdbasalfacq	-0.000133194	-0.0009	-0.003	-0.000252939	-0.000252939	-0.000252939
	gdbasalfac	0.001470654	0.0056	0.03	0.006578208	0.006578208	0.006578208
	gdbasalconst	-0.805581404	-1.01	-1.98	-1.319846682	-1.319846682	-1.319846682
	gdbreastfacq	-0.000133194	-0.0009	-0.003	-0.000252939	-0.000252939	-0.000252939
	gdbreastfac	0.001470654	0.0056	0.03	0.006578208	0.006578208	0.006578208
	gdbreastconst	-0.805581404	-1.01	-1.98	-1.319846682	-1.319846682	-1.319846682
	dbasalheightalloslope	42.88	42.88	42.88	42.88	42.88	42.88
	dbasalheightalloexp	1	1	1	1	1	1
	dbreastheightalloslope	42.88	42.88	42.88	42.88	42.88	42.88
	dbreastheightalloexp	1	1	1	1	1	1
	dbasalheightslopenonlin	44.43163	44.43163	44.43163	44.43163	44.43163	44.43163
	dbreastheightslopenonlin	7.02	7.02	7.02	7.02	7.02	7.02
	mortbg	0.0001	0.0001	0.0001	0.0001	0.0001	0.0001
	maximumage	609	500	500*	250	250	250
	mortage	8.18785	8.18785	8.18785	8.18785	8.18785	8.18785
	mortyouth	0.762855	0.762855	0.762855	0.762855	0.762855	0.4
	mortyouthinfluenceexp	0.79295	0.79295	0.79295	0.79295	0.79295	0.79295
	mgrowth	0.5	0.5	0.5	0.5	0.5	0.01
	mdensity	0.5	0.5	0.5	0.5	0.5	0.2
	densityvaluemaximumatheight	0	0	0	0	0	0
	mweather	0.1	0.1	0.1	0.1	0.1	0.1
	heightweathermorteinflussexp	0.2	0.2	0.2	0.2	0.2	0.2
	mdrought	0.237805	0.237805	0.237805	0.1	0.1	0.5
	seedconemort	0.44724	0.44724	0.44724	0.44724	0.44724	0.44724
	seedfloormort	0.55803	0.55803	0.55803	0.55803	0.55803	0.999
	seedmaxage	4*	1*	1*	1	1	1
	janthresholdtemp	-45	-33	-60	-33	-33	-33
	janthresholdtempcalcvalue	9	6.6	9	6.6	6.6	6.6
	weathervariablea	0.078	0.163	0.078	0.163	0.163	0.163
	weathervariableb	14.825	12.319	14.825	12.319	12.319	12.319
	weathervariablec	0.108	0.168	0.108	0.168	0.168	0.168
	weathervariabled	0.1771	0.305	0.1771	0.305	0.305	0.305

Appendix C. CryoGrid model parameters and constants used

Table C1. Overview of the CryoGrid parameters used.

Process / Parameter		Value	Unit	Source
Density falling snow	ρ_{snow}	100 (SPA), 200 (NYU/KHA)	kg m^{-3}	Stuenzi et al. (2021a)
Albedo ground	α	0.3	-	Stuenzi et al. (2021a)
Roughness length	z_0	0.001	M	Westermann et al. (2016)
Roughness length snow	$z0_{snow}$	0.0001	M	Boike et al. (2019)
Geothermal heat flux	F_{lb}	0.05	W m^{-2}	Westermann et al. (2016)
Thermal cond. mineral soil	$k_{mineral}$	3.0	W m^{-1} K^{-1}	Westermann et al. (2016)
Emissivity		0.99	-	Langer et al. (2011)
Root depth		0.2	M	Stuenzi et al. (2021a)
Evaporation depth		0.1	M	Nitzbon et al. (2019)
Hydraulic conductivity		10-5	m s^{-1}	Boike et al. (2019)

Appendix D. Spatial distribution of the leaf area index (LAI) for mixed species and pure species simulations at the focus regions in 5-year steps.
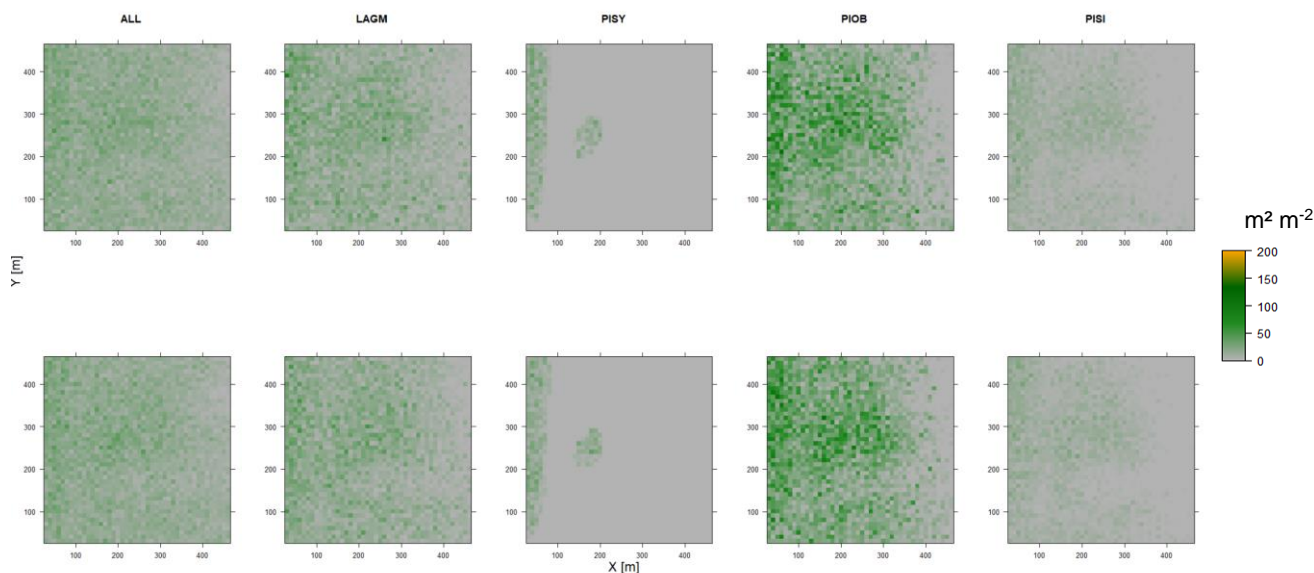
Figure D1. Leaf area index (LAI) values of the CryoGrid-grid aggregated at year 2015 at Lake Khamra. Upper row LAVESI-CryoGrid coupled; lower row LAVESI simulations. LAGM *Larix gmelinii*; PIOB *Picea obovata*; PISI *Pinus sibirica*; PISY *Pinus sylvestris*.
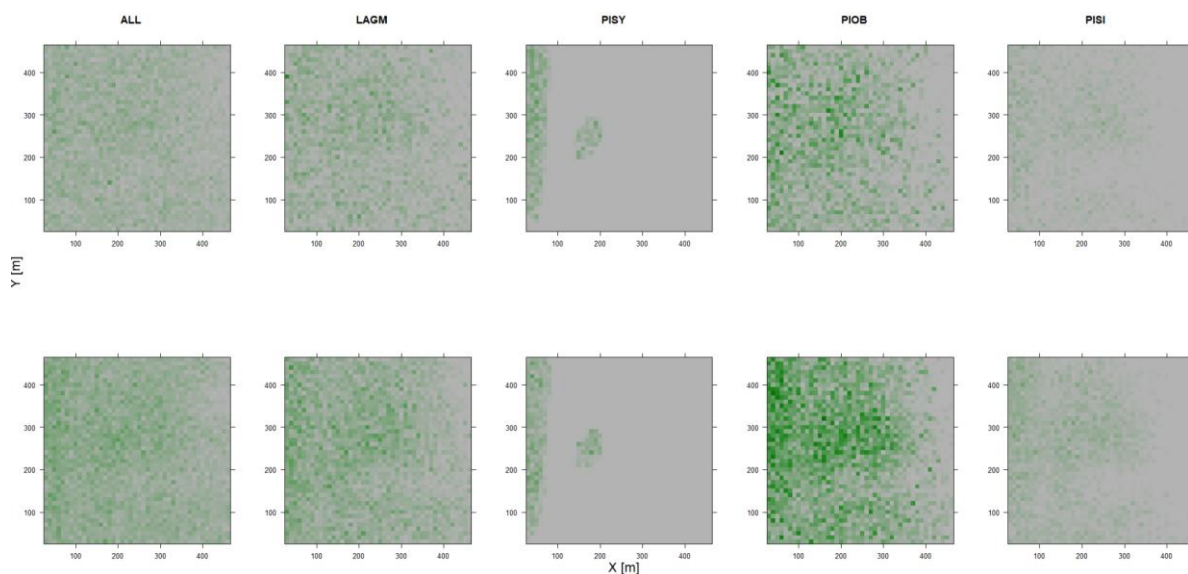
Figure D2. Leaf area index (LAI) values of the CryoGrid-grid aggregated at year 2020 at Lake Khamra. Upper row LAVESI-CryoGrid coupled; lower row LAVESI simulations. LAGM *Larix gmelinii*; PIOB *Picea obovata*; PISI *Pinus sibirica*; PISY *Pinus sylvestris*.
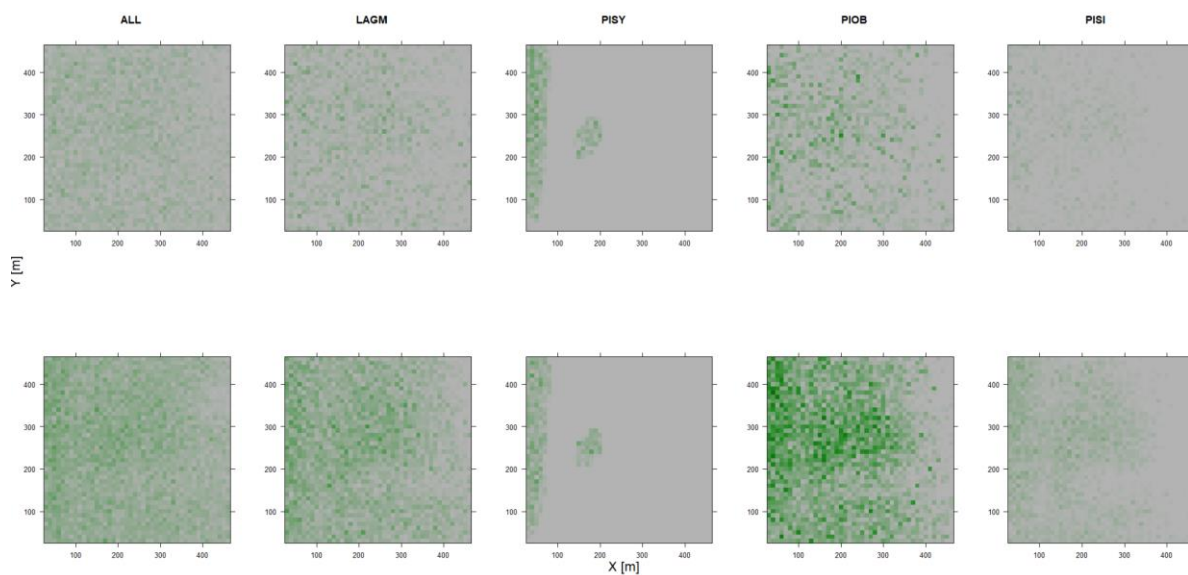
Figure D3. Leaf area index (LAI) values of the CryoGrid-grid aggregated at year 2025 at Lake Khamra. Upper row LAVESI-CryoGrid coupled; lower row LAVESI simulations. LAGM *Larix gmelinii*; PIOB *Picea obovata*; PISI *Pinus sibirica*; PISY *Pinus sylvestris*.
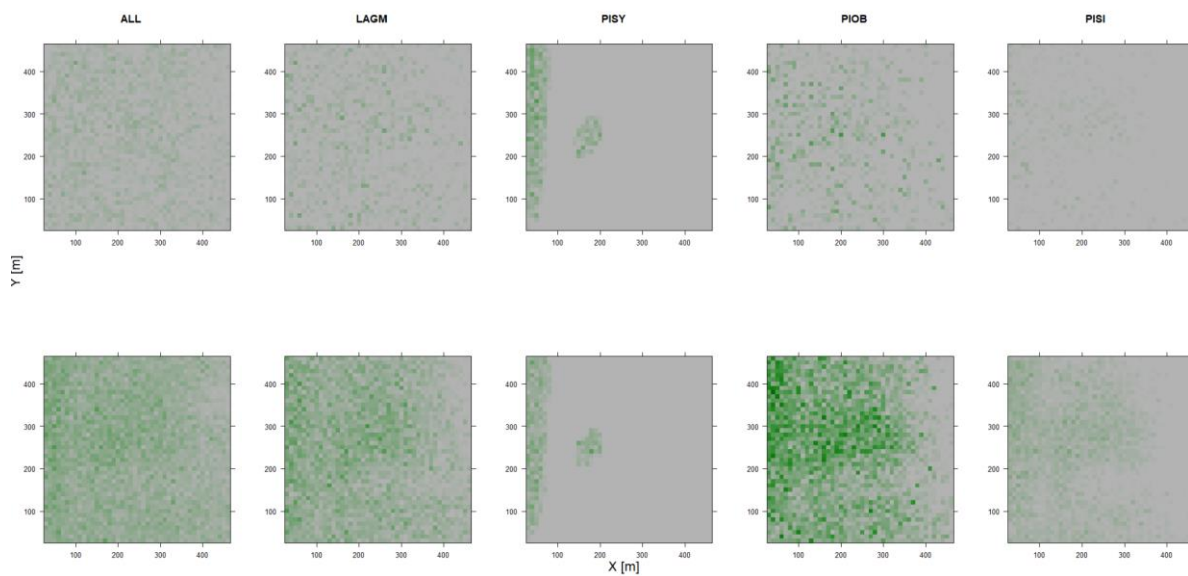
Figure D4. Leaf area index (LAI) values of the CryoGrid-grid aggregated at year 2030 at Lake Khamra. Upper row LAVESI-CryoGrid coupled; lower row LAVESI simulations. LAGM *Larix gmelinii*; PIOB *Picea obovata*; PISI *Pinus sibirica*; PISY *Pinus sylvestris*.
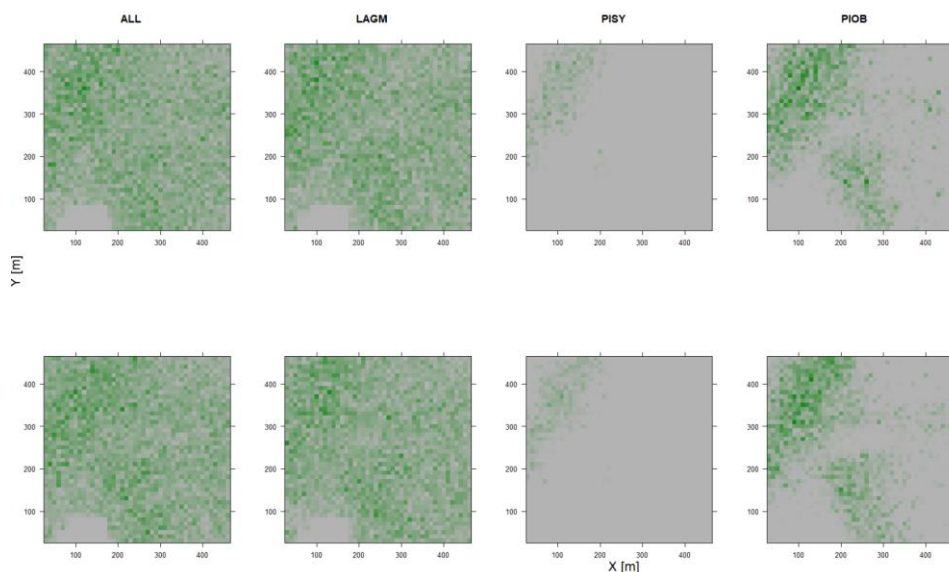
Figure D5. Leaf area index (LAI) values of the CryoGrid-grid aggregated at year 2015 at Nyurba. Upper row LAVESI-CryoGrid
coupled; lower row LAVESI simulations. LAGM *Larix gmelinii*; **PIOB** *Picea obovata*; **PISI** *Pinus sibirica*; **PISY** *Pinus sylvestris*.
Simulations with PISI were not possible.
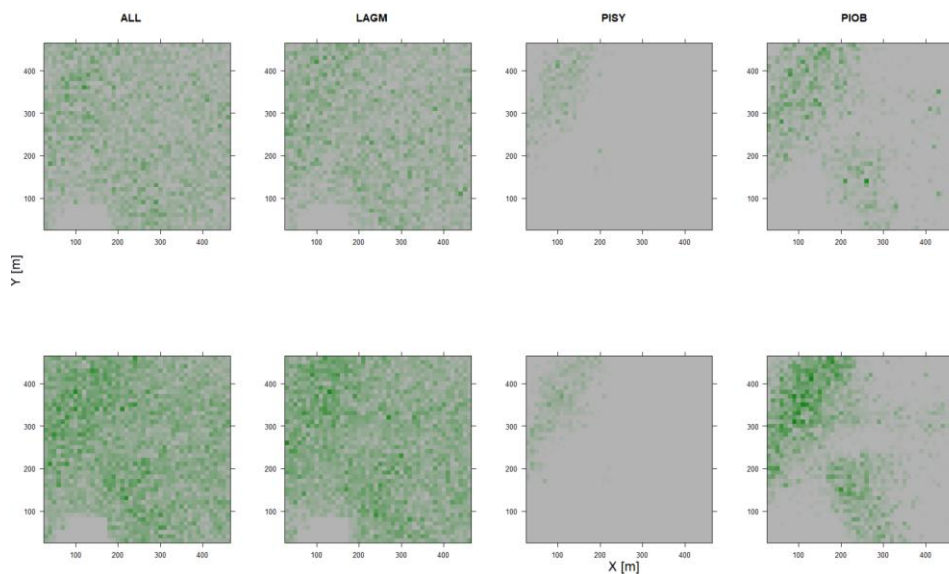
Figure D6. Leaf area index (LAI) values of the CryoGrid-grid aggregated at year 2020 at Nyurba. Upper row LAVESI-CryoGrid
coupled; lower row LAVESI simulations. LAGM *Larix gmelinii*; **PIOB** *Picea obovata*; **PISI** *Pinus sibirica*; **PISY** *Pinus sylvestris*.
Simulations with PISI were not possible.
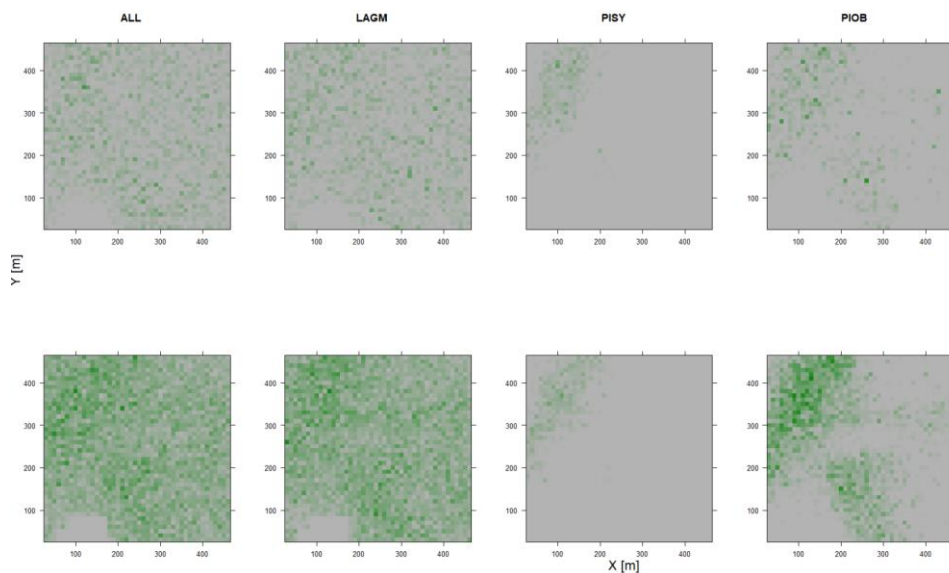
Figure D7. Leaf area index (LAI) values of the CryoGrid-grid aggregated at year 2025 at Nyurba. Upper row LAVESI-CryoGrid coupled; lower row LAVESI simulations. LAGM *Larix gmelinii***; PIOB** *Picea obovata***; PISI** *Pinus sibirica***; PISY** *Pinus sylvestris***. Simulations with PISI were not possible.**
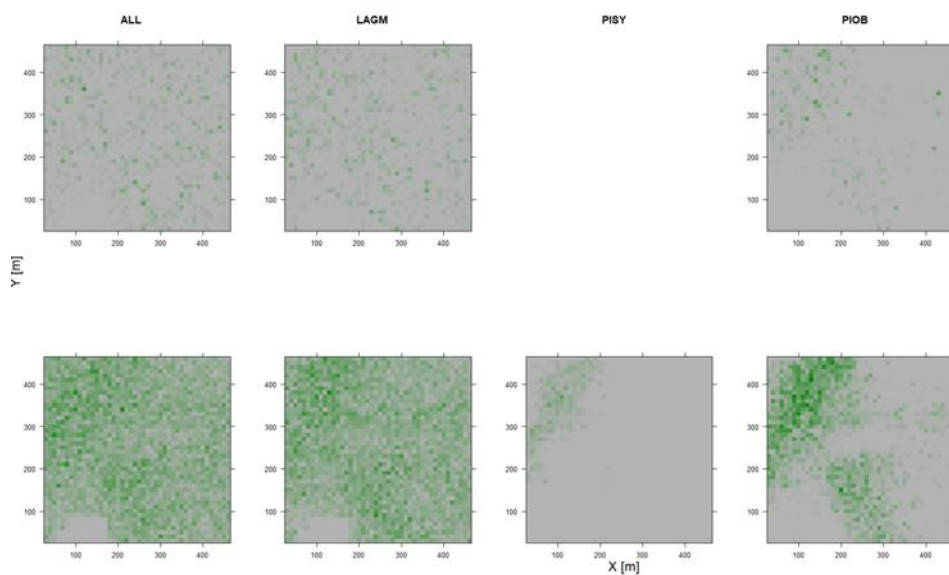
Figure D8. Leaf area index (LAI) values of the CryoGrid-grid aggregated at year 2030 at Nyurba. Upper row LAVESI-CryoGrid coupled; lower row LAVESI simulations. LAGM *Larix gmelinii***; PIOB** *Picea obovata***; PISI** *Pinus sibirica***; PISY** *Pinus sylvestris***. Simulations with PISI and PISY coupled were not possible.**
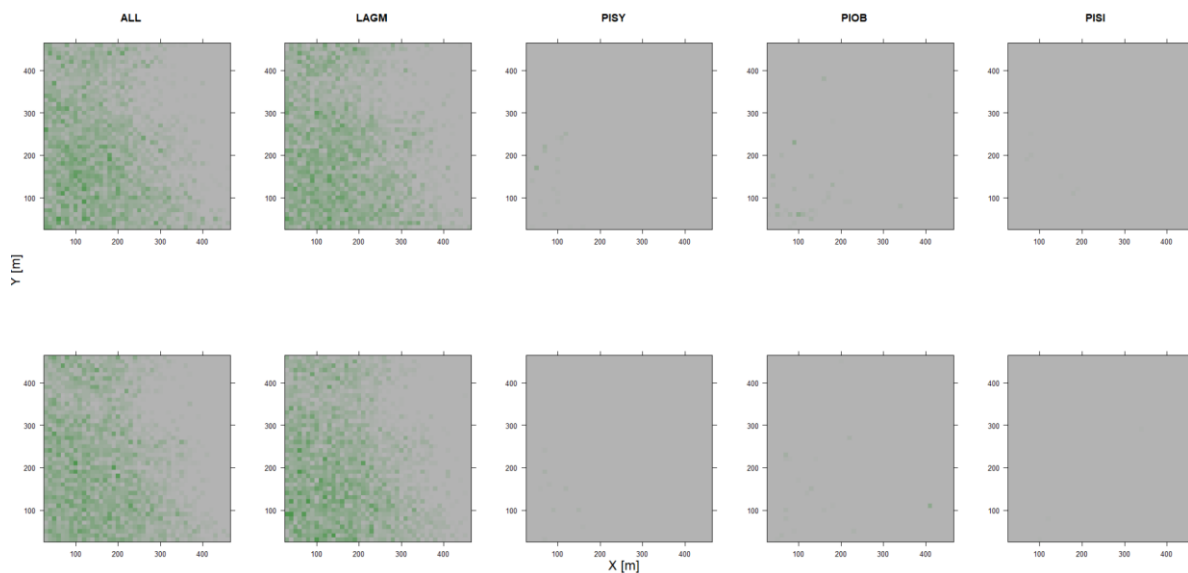
Figure D9. Leaf area index (LAI) values of the CryoGrid-grid aggregated at year 2015 at Spasskaya Pad. Upper row LAVESI-CryoGrid coupled; lower row LAVESI simulations. LAGM *Larix gmelinii*; PIOB *Picea obovata*; PISI *Pinus sibirica*; PISY *Pinus sylvestris*.
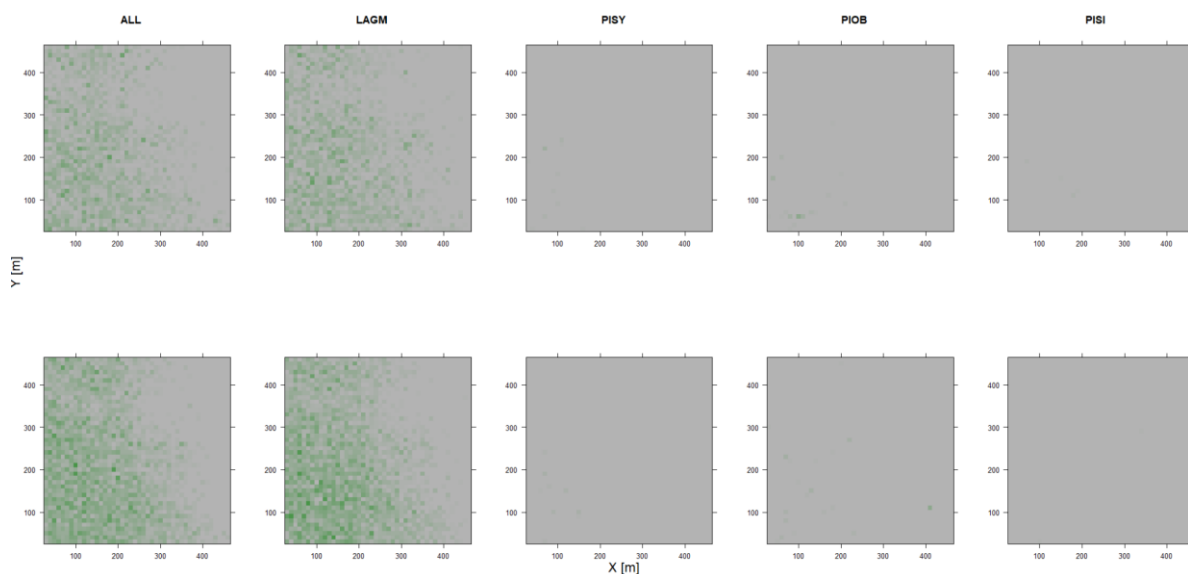
Figure D10. Leaf area index (LAI) values of the CryoGrid-grid aggregated at year 2020 at Spasskaya Pad. Upper row LAVESI-CryoGrid coupled; lower row LAVESI simulations. LAGM *Larix gmelinii*; PIOB *Picea obovata*; PISI *Pinus sibirica*; PISY *Pinus sylvestris*.
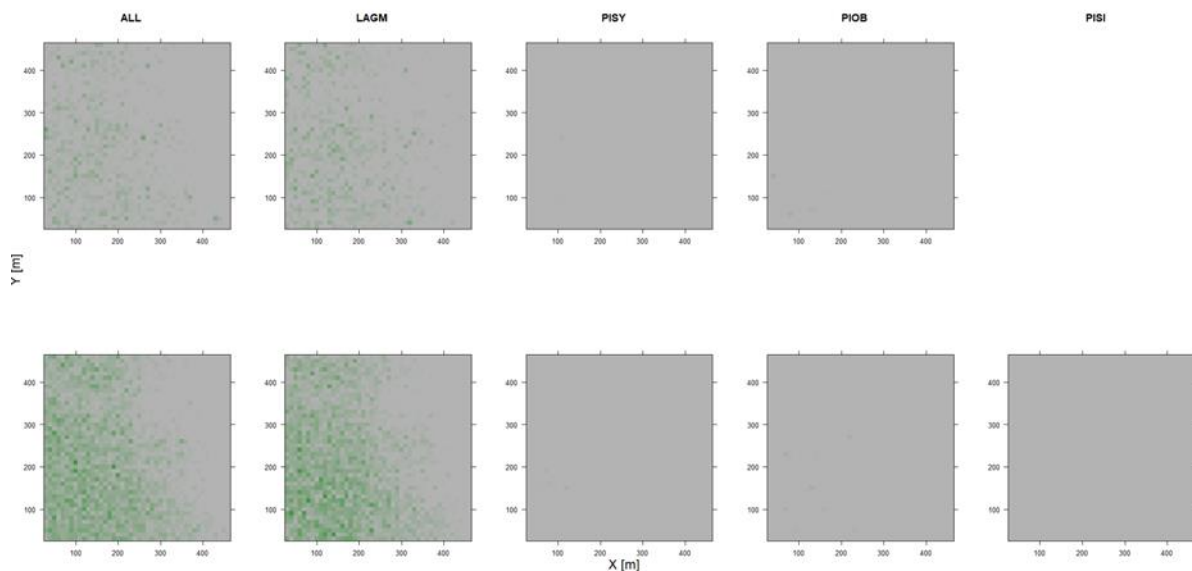
Figure D11. Leaf area index (LAI) values of the CryoGrid-grid aggregated at year 2025 at Spasskaya Pad. Upper row LAVESI-CryoGrid coupled; lower row LAVESI simulations. LAGM *Larix gmelinii*; PIOB *Picea obovata*; PISI *Pinus sibirica*; PISY *Pinus sylvestris*. Simulations with PISI coupled was not possible.
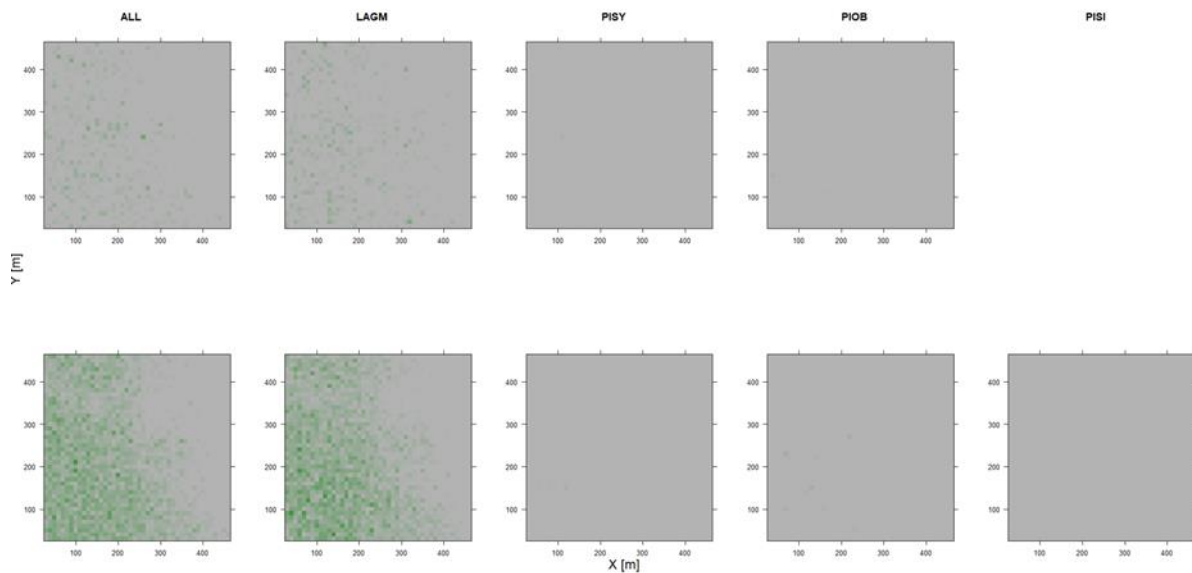
Figure D12. Leaf area index (LAI) values of the CryoGrid-grid aggregated at year 2030 at Spasskaya Pad. Upper row LAVESI-CryoGrid coupled; lower row LAVESI simulations. LAGM *Larix gmelinii*; PIOB *Picea obovata*; PISI *Pinus sibirica*; PISY *Pinus sylvestris*. Simulations with PISI coupled was not possible.

Appendix E. Evolution of Leaf Area Index (LAI) across the focus region simulation areas
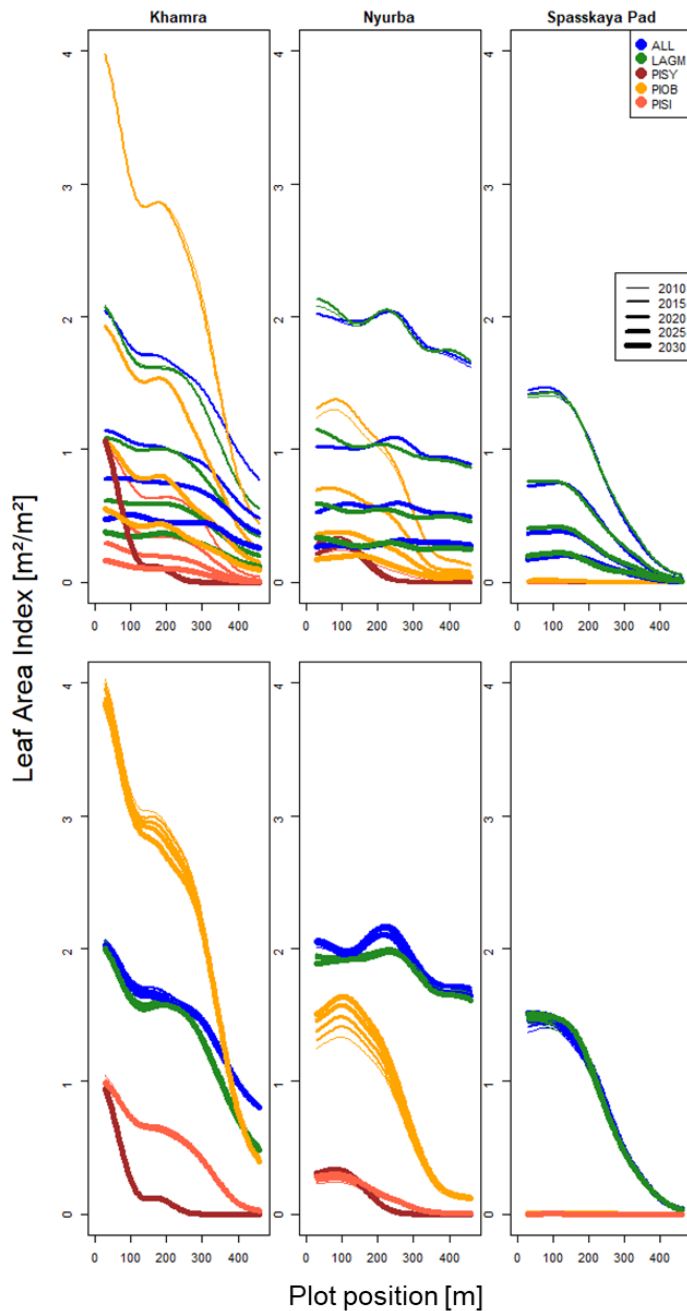
Figure E1. Mean leaf area index aggregated east-west for each simulated focus area and time slice (2010–2030). Upper row LAVESI-CryoGrid coupled version; lower row only LAVESI.